ANALYSIS OF TORQUE VECTORING SYSTEMS THROUGH TIRE AND VEHICLE MODEL SIMULATION

A Thesis

Presented to

The Graduate Faculty of The University of Akron

In Partial Fulfillment

of the Requirements for the Degree

Master of Science

Christopher Chatfield

August 2023

ANALYSIS OF TORQUE VECTORING SYSTEMS THROUGH TIRE

AND VEHICLE MODEL SIMULATION

Christopher Chatfield

Thesis

Approved:

_____
Advisor
Dr. Daniel Deckler

_____
Committee Member
Dr. Alper Buldum

_____
Committee Member
Dr. Ajay Mahajan

Accepted:

_____
Department Chair
Dr. Sergio Felicelli

_____
Dean of the College of
Engineering and Polymer Science
Dr. Craig Menzemer

_____
Dean of the Graduate School
Dr. Suzanne Bausch

_____
Date

ABSTRACT

With advancements in modern battery technology, electric vehicles (EVs) have become increasingly more prevalent on the road. While the technology is still evolving, it has become clear that EVs have numerous benefits, and some of which are performance oriented. One of these benefits is the ability to package electric motors that are directly connected to individual wheels or axles. With this, combined with the considerably reduced feedback loop of electric motors with respect to a combustion engine, it has become easier to implement advanced motor control systems, such as traction control (TC) and torque vectoring (TV).

In this thesis, a simulation model was created by building torque vectoring algorithms into Milliken Moment Diagram (MMD) calculations for specified tire and vehicle parameters. In which, the cornering response of a given vehicle will be calculated given a set of input conditions. Various motor configurations were simulated in these MMDs to compare the differences in vehicle behavior to demonstrate the benefits of torque vectoring. After simulating the motor configurations, the results indicate that TV can significantly improve yaw behavior, especially when all wheels are contributing. Several input conditions were also varied to explore the robustness of the models, in which a TV control

“map” is created and applied to show how the model can be utilized as a tool to improve vehicle performance in coordination with testing.

DEDICATION

I would like to dedicate this thesis to my wonderful family, and I am grateful for their immense support which helped me achieve this goal. My father, the inspiration behind me pursuing engineering and his work ethic and initiative make him an amazing role model. My mother, who raised me to be the best that I can be and has provided invaluable support through all of life's hurdles. Lastly, my sister, Caroline, a great friend, and the best sister I could ask for.

ACKNOWLEDGEMENT

I would like to thank Michael Arbogast and Michael Stackpole at Stackpole Engineering for helping navigate the intricacies of tire modeling. Their wealth of knowledge and generosity have helped this thesis come to fruition, which is greatly appreciated.

I thank the University of Akron FSAE teams, both combustion and electric, for working with me on this endeavor. Their patience and willingness to collaborate throughout this project has not gone unnoticed. I would also like to thank my advisor, Dr. Daniel Deckler, for his assistance both with the design teams and keeping me on track to finish this project. I thank both Dr. Alper Buldum and Dr. Ajay Mahajan for their time reviewing my thesis as members of my committee.

Lastly, I would like to thank Mustafa Malik, a friend and fellow master's student, who gave me direction and assistance countless times throughout this project. Without his guidance, it would have been a monumental challenge to gather the resources to complete the thesis.

TABLE OF CONTENTS

Page

LIST OF FIGURES

Figure Page

LIST OF TABLES

CHAPTER I

BACKGROUND

The contemporary study of vehicle dynamics came to fruition in the 1930's, in which significant progress and standardization was made in the next few following decades. The fundamentals of vehicle dynamics are covered in [1-6]. In particular, [1] focuses on the motorsport applications and introduces the MMD's used in this thesis. Early concepts of the MMD can be found in [7], with the MMD itself originating in [8], and being refined in [9]. The equations comprising MMDs are explained in detail in [10], in which the MMD code for this thesis is built upon.

Supplementing the progression of vehicle dynamics studies, the parameterization of tires was developed as tires play a pivotal role in vehicle behavior. The Pacejka tire model has become the standard to parameterize tires for vehicle simulations. The predecessor to the tire model [11] was a simpler set of nondimensionalized scalars. In the 1980s, the Magic Formula [12] was created which became the standard of tire modeling moving forward, with further developments such as lateral/longitudinal slip [13] and normalization parameters [14] as subsequent improvements. [15-17] cover the equations used in modern tire models such as the one used in this thesis, and how they are applied.

The benefits from conducting this thesis are twofold. Primarily, such an adaptation of a vehicle model that incorporates tire modeling and MMD's for TV is not publicly available. This is intended to serve as a tool for FSAE students. In addition, it should prove useful to many other transportation research and development projects, as the inputs are modifiable and scalable. Secondly, using the model to vary conditions is intended to validate the notion that TV will enhance vehicle cornering behavior. This will also quantify how much cornering performance is improved while adding TV.

Coordinate Systems and Reference Frames

There are three coordinate frames that must be established for the simulation. The first two have the vehicle center of mass as the origin. The vehicle coordinates used are Z-down, per SAE J670 standards [20]. Thus, the positive Z-direction is pointing downwards. The first coordinate frame is called the "body frame", in which the positive X direction always faces towards the front of the vehicle body, and positive Y direction faces the right side of the vehicle. Each moment follows the right-hand rule, so the yaw moment (MZ) is pointed clockwise, looking top down at the vehicle. Figure 1 below shows the front and top views of the body-frame coordinates in relation to the vehicle.

The second coordinate system used is the "velocity frame". It is configured similarly to the body frame; however, the difference is that the positive X direction is rotated with respect to the vehicle slip angle (β). In this case, the positive X coordinates are in the direction of travel of the vehicle, which will differ

from facing the front of the vehicle if vehicle slip is nonzero. Figure 2 below illustrates this coordinate frame in relation to the vehicle orientation.

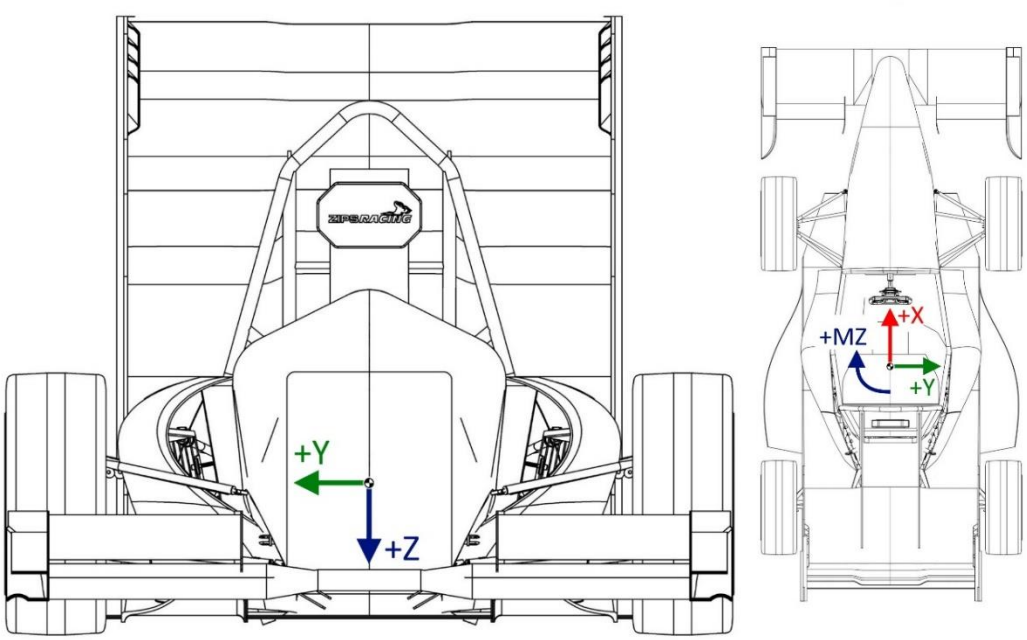

Figure 1: Front and Top Views of the vehicle in body-frame coordinates

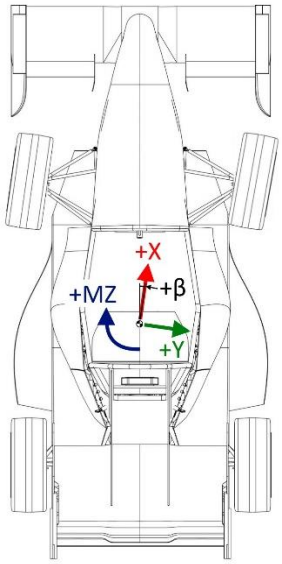

Figure 2: Top View of the vehicle in velocity-frame coordinates

The final coordinate frames to consider are those of each wheel of the vehicle. The axes are oriented akin to that of the body frame, except they are aligned with the direction of travel of each respective wheel. This means that, for the front wheels, each frame rotates about the Z-axis with the steering angle. Figure 3 below, derived from [21], depicts how the coordinates are oriented with respect to wheel travel and slip. Two different coordinate frames are shown in this figure, one being the wheel center (blue), and the other being the tire contact patch (red). The frames being used in the calculations are those of the tire contact patches since that is where the vehicle forces are being generated.

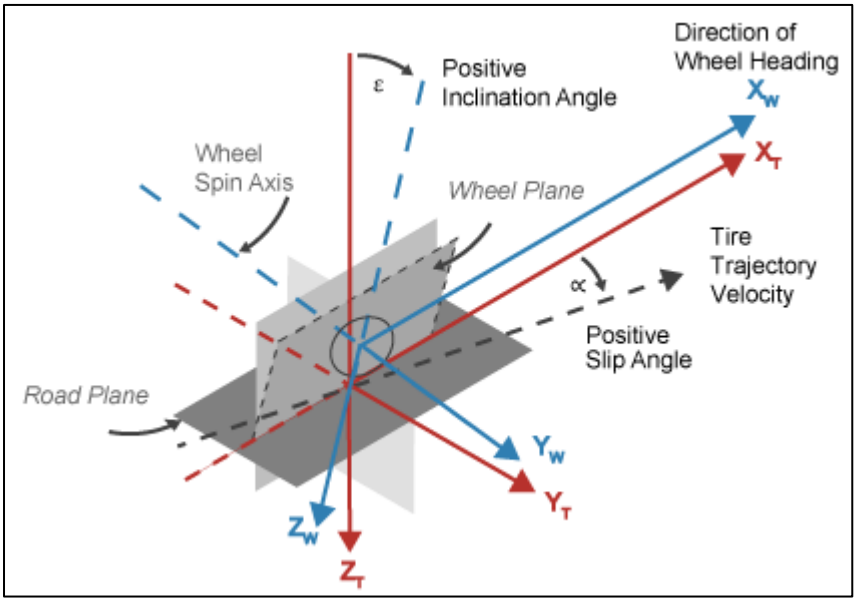

Figure 3: Individual wheel coordinate system, axes, and angles (Mathworks)

Torque Vectoring (TV) Overview

In the simplest sense, torque vectoring (TV) is considered any method which actively distributes power to individual wheels to enhance the behavior of a vehicle. TV systems are configured to optimize longitudinal grip on individual tires. Typically, the goal is to increase the vehicle's yaw (MZ) rate capabilities without significantly hampering longitudinal (X) and lateral (Y) accelerations. When cornering, this can be achieved by increasing torque to the wheels on the outside of the corner and decreasing torque to the inside wheels.

TV has been in use in non-automotive vehicles, such as smaller robots and zero-turn mowers for decades prior to being widely adopted in automotive applications [22], [23]. Many of these applications involve the variation in motor torque being the sole method of steering, as it is mechanically simpler than designing a steering system. The earliest implementations of torque vectoring in automobiles utilized mechanical differentials that were able to vary the torque distribution to individual output shafts. This is typically achieved hydraulically or electronically, and results in an additional system that significantly increases cost, complexity, and weight of the vehicle.

Another adaptation of torque vectoring comes from actuating individual brakes to apply negative torque to the inside wheels, called "brake torque vectoring". This allows for a system that is mechanically no different than a vehicle without TV, as the same brake system is retained. Thus, it is favorable from a simplicity and cost standpoint. The major drawback to this kind of system is that kinetic energy is unrecoverably expelled from the vehicle to increase yaw.

This system also induces additional heat and fatigue in the braking system that must be factored as a design consideration. This configuration was not initially possible on road cars, due to laws prohibiting electronically controlled braking systems. However, in the past decade, it has been made possible and adopted as the most common instance of individual wheel torque control due to its simplicity.

With the advent of electric motors, a much more effective method of TV has begun to emerge when each wheel is individually controlled by a motor. Through direct torque control of the motors, TV can be controlled with significantly higher precision, and the traction of each tire is closer than ever to be optimized. Furthermore, with the energy recovery capabilities of electric motors, it is now possible to apply negative torque to a wheel, up to the peak torque of the motor, which mitigates the drawbacks of brake torque vectoring. The simulations conducted utilize this method of torque vectoring through individual motor control.

CHAPTER II

VEHICLE PARAMETERS

The vehicle to be simulated is compliant with the Formula SAE (FSAE) rulebook under the EV class. FSAE is a competition for engineering students to design and build a Formula-style race car on an annual basis, with competitions held internationally. Despite the competition being primarily hailed as a learning experience for the students involved, the vehicles entered are remarkable feats of engineering. A few FSAE vehicles have even broken overall records in 0-60mph (0-100kph) acceleration runs. This is in part due to the FSAE rulebook being quite “open” in comparison to other forms of professional motorsport, such as Formula 1, to inspire more creativity and freedom in design.

The vehicle in the simulation is intended to be an example representing a competitive FSAE car as proof of concept, and it is not meant to be an exact replica of an existing car, or one currently being designed or built. That said, the simulation code is designed inherently so that vehicle and tire parameters can be easily altered. This means that the simulation created can be scaled to any given passenger vehicle with four wheels.

The simulated vehicle has a weight of 300kg (661lb), wheelbase of 1.53m (5.02ft), and a track width of 1.22m (4.00ft). The height of the center of gravity of the vehicle is 0.295m (0.97ft). Statically, the vehicle’s weight is distributed

symmetrically left to right, and 49% on the front. 30mph (13.4m/s) was selected as the nominal speed, as that is the average speed in which a Formula SAE vehicle is traveling throughout an autocross course.

Powertrain Selection

The powertrain package selected for the vehicle is the AMK A2370DD, an in-wheel motor and inverter package that is specifically tailored to the FSAE rulebook and is the most common competitive powertrain package in FSAE. More detailed motor data can be found in [24]. The maximum bus voltage allowed per the FSAE rulebook is 600 VDC, so the motor data respective to this voltage was used in the simulation. For a single motor, the peak power is 35kW (46.9HP), and the peak torque is 21Nm (15.5 ft-lb). The characteristic speed of the motor at 600Vdc bus voltage is 16,000 RPM. At this speed, peak power is achieved. Below the characteristic speed, the motor's maximum torque of 21Nm is held constant. Figures 4 and 5 below show the torque and power characteristics of the motor, with Figure 5 zoomed in on the power and torque curves at and above the characteristic speed.

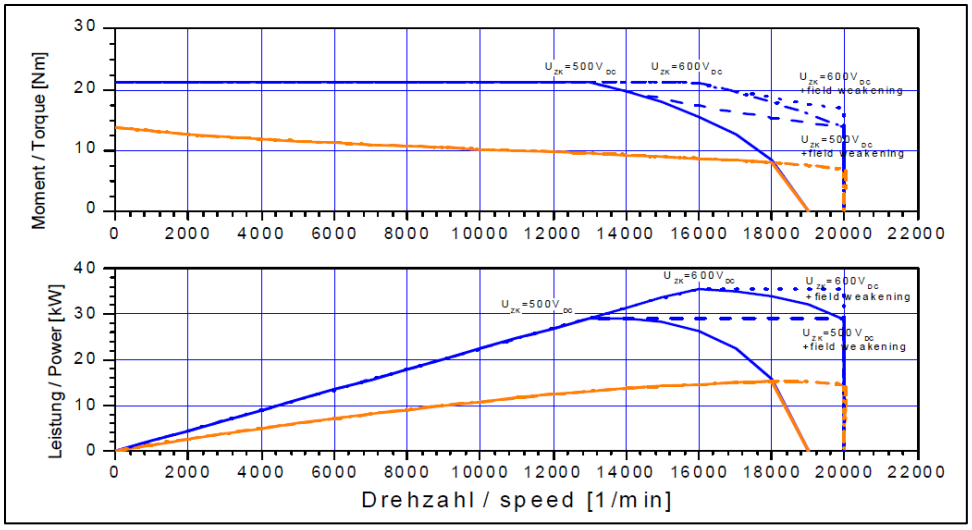

Figure 4: Performance Characteristics of AMK A2370DD (AMK)

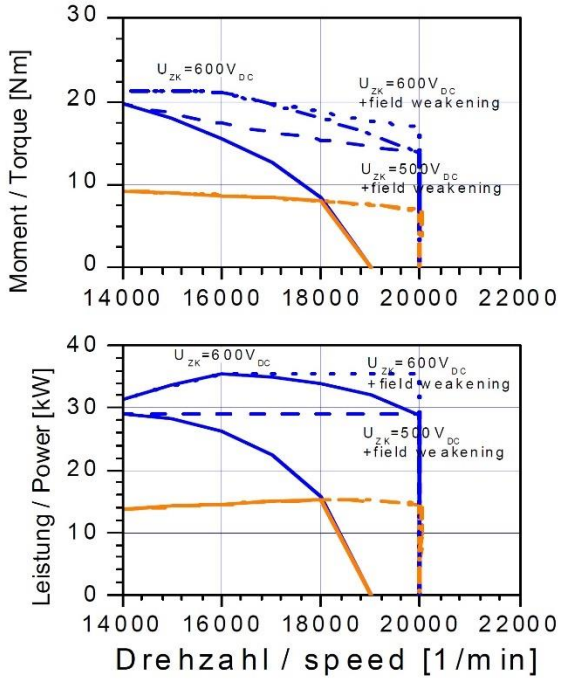

Figure 5: Motor Torque and Power curves at and above characteristic speed (AMK)

Something noteworthy is that while the rulebook specifies the vehicle's power output must not exceed 100kW at any given moment, the motors

individually can produce 35kW at peak. If all four motors are operating at their peak, this would glaringly exceed this 100kW limit. However, what this does allow is a higher level of torque vectoring for each motor if they are being individually controlled.

The gearboxes are essential to consider in tandem with the motor selection. The vehicle would not make the most of the motors if they were directly connected to the wheels. A single-speed planetary gearbox is the most ubiquitous solution, as they can be packaged on each corner coupled to the motor. In this simulation, a 10:1 final drive ratio in the gearbox is used, which amplifies the peak torque for each motor to 210Nm. The 10:1 ratio was selected after analyzing track data from previous vehicles to estimate a final drive with the same theoretical maximum speed. Factoring in the 10:1 gear ratio and 20” diameter tires, the 16,000rpm characteristic speed would be reached at 42.6m/s (95.2mph). In addition, the 100kW limit would be reached by all four motors if the vehicle was traveling at 30.2m/s (67.5mph). Thus, it can be assumed that the torque output would not be saturated during most instances of cornering.

In total, there were five motor configurations considered in this study. Configuration (i) was a simple dual-motor rear-wheel drive (RWD) setup without torque vectoring as a benchmark. Configurations (ii) and (iii) were also RWD, however they implement two different methods of torque vectoring. The motors in (ii) only increase torque to the rear wheel on the outside of the corner, while (iii) applies both positive torque to the outside wheel, and negative torque (regenerative braking) to the inside wheel. Applying regen to the inside wheel

will reduce longitudinal thrust but has advantages when considering the yaw rate of the vehicle. Configurations (iv) and (v) are all-wheel drive (AWD), in which all four wheels have individual motors. Similarly respective to (ii) and (iii), motors in (iv) apply only positive torque, and (v) can distribute both positive torque and regen to individual motors. In addition, both AWD configurations used for comparison have a 50/50 front/rear torque bias. Figure 6 below visualizes the differences between all described configurations, respectively with (i) on the left, and (v) on the right.

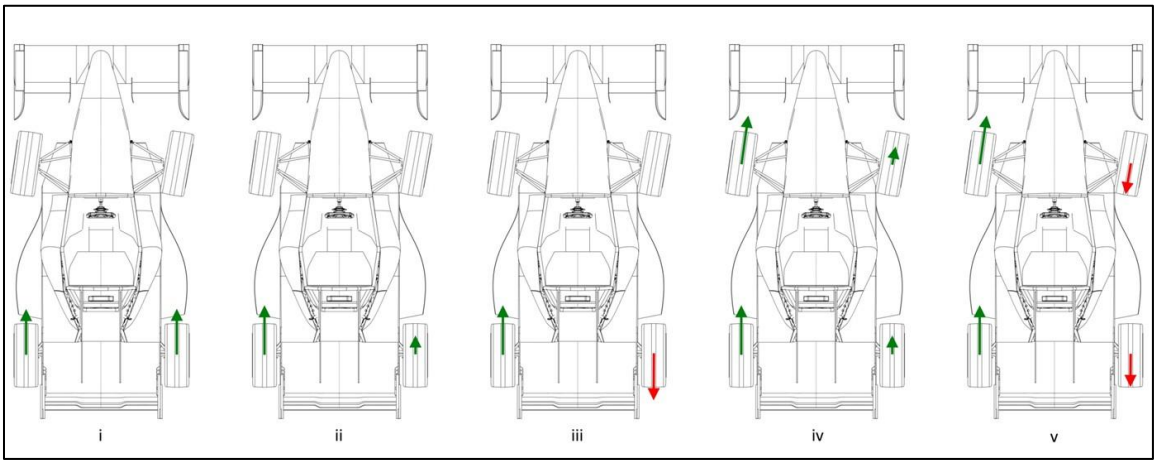

Figure 6: Visualization of motor TV configurations to be analyzed

Another parameter to consider with a torque vectoring system is the management of inputs and outputs. For active torque vectoring systems, vehicle data is collected through driver input sensors, accelerometers, and speed sensors. In the simulated vehicle, the only sensors are the throttle position, brake pressure, and steering position sensors. Similarly, the output commanded torques to each motor is linear based on steering and throttle position. The main

reason behind simplifying the input and output complexity is to provide a system that is simple and easily replicable, yet still retains the fundamentals of a functional torque vectoring system. Another benefit to a simple linear system is that it will be more controllable and predictable for the driver. Adapting to the increased performance of a vehicle with TV will already be a learning curve, so having a linear system is an ideal first step, despite some optimization being left on the table.

The scaling factor of TV intensity is set based on a range of typical steering angles seen in vehicle data on track. For a benchmark, the steering angle in which TV reaches its maximum is set to 10 degrees. In the case of zero throttle or braking input, the outside motors will linearly increase torque up to their max when steering input is increased up to 10 degrees. Thus, the scaling factor will be set to 21Nm per degree of steering. In the cases where there is regen, the inside motors will similarly apply negative torque with this factor applied. Beyond 10 degrees, the TV will plateau at its maximum. Figure 7 below shows how much torque is added to the torque command of an outside motor based on steering angle. This factor was set at 10 degrees as a compromise to have enough of an impact with smaller steering inputs, but not reach its peak too abruptly. It is advised that the vehicle should have a dial for the driver to adjust TV factor, like how traction control intensity and brake bias is typically handled. This will allow the vehicle to better adapt to changes such as the surface grip, and track layout. After initial simulation is complete, a “map” going into greater

detail on the motor outputs based on throttle and steering position will be constructed in Chapter V.

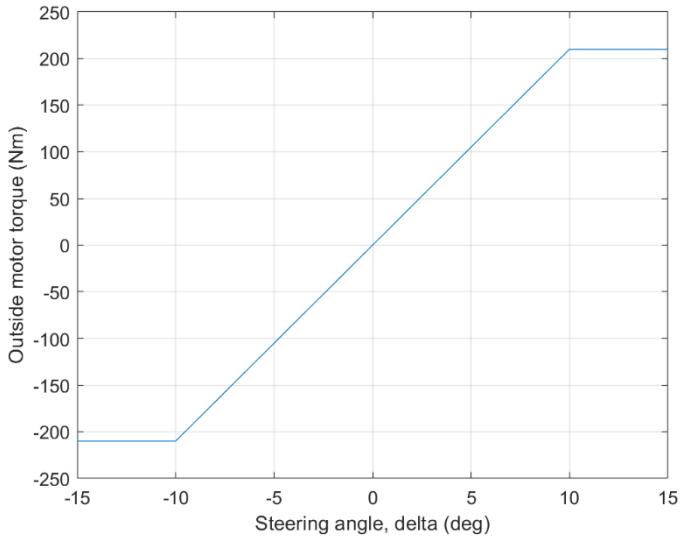

Figure 7: Outside motor TV output versus steering angle, without throttle input

Aerodynamic Considerations

Another aspect to consider is that most of the advanced FSAE teams utilize aerodynamic devices, such as wings and diffusers, to increase normal force to the tires for higher grip levels at racing speeds. Computational fluid dynamic (CFD) simulations computing the lift and drag properties of the vehicle can be applied to further improve accuracy in this simulation. Since the vehicle being simulated does not have a simulated aero package, a simplified model from a similar FSAE vehicle was applied. At 48.3kph (30mph), the vehicle produces 182N of downforce on the front axles, and 285N of downforce on the

rear axles. Downforce can then be estimated at any given speed by fitting a square equation through that data point and 0N at 0kph. The downforce equations become as follows, with downforce in Newtons, and velocity in meters/second.

$$DF_f = 1.011{V_x}^2 \quad [1]$$

$$DF_r = 1.586{V_x}^2 \quad [2]$$

CHAPTER III

TIRE MODELING AND SELECTION

Tire modeling is the characterization of a tire simplified into coefficients. Regarding computational efficiency, tire models are an effective solution to parameterize tire forces and moments given certain inputs. The data is produced by indoor tire test machines, then fitted using proprietary tire modeling software to generate the coefficients. Appendix A comprises the model coefficients and the equations used to decode them for use in simulation.

For Formula SAE, there is no restriction on the tire selections in the rulebook, such that no other rules are violated. However, there are tires specifically designed to work with the scale and dynamics of FSAE vehicles. The FSAE Tire Test Consortium (TTC) is an organization which manages a library of force & moment (F&M) test data of these tires for teams to use. The consortium data can be found populated in [25]. To ensure standardization, all the tires are tested at the Calspan test labs, and data is analyzed by Stackpole Engineering.

The tire spec chosen for this vehicle is the Goodyear D2704. This is in part due to the availability of the data on this tire on the TTC. This tire has also been run historically by the University of Akron FSAE teams, so its characteristics are well understood. The size of the tire selected is 20.0 x 7.0 – 13, and it will be run on a 13x7 wheel. 13 psi was selected as a baseline tire

pressure and is assumed to be constant. These parameters are used to select the specific tire model file used in the simulation.

The tire model output file that is processed is a .TIR file, in which there are different versions and types of models to consider. The classification “use mode” dictates how many scenarios were included in the model. For example, the model used follows the PAC2002 format, and is classified as use mode 4. The inputs of the model are normal force (Fz), wheel velocity (Vx), inclination angle (γ), lateral slip angle (α), and longitudinal slip (κ). Use mode 4 means the tire model will output forces in the X and Y directions, and moments in the X, Y, and Z directions. In addition, the model can output forces & moments in combined lateral and longitudinal slip conditions. The D2704 is a bias-ply tire, therefore the tire model will have to account for asymmetrical tire behavior as a result. Since the modeled tire was oriented on the right-hand side during testing, the models on the left-hand side of the vehicle will be inverted laterally.

A use mode 4 PAC2002 tire model consists of ninety-six coefficients which are applied in nonlinear equations to calculate output forces and moments. The equations are from the MF-Tyre manual and can be referenced in Appendix A. Reference conditions and scaling factors are also included in the .TIR file. Due to the complex nature of tire behavior, the output forces and moments are fit using equations combined sinusoids and exponentials in many cases.

CHAPTER IV

MILLIKEN MOMENT DIAGRAM (MMD) OVERVIEW

To simulate the yaw behavior of the vehicle, a Milliken Moment Diagram (MMD), also called a Yaw Moment Diagram (YMD), was created in the code. An MMD serves many purposes in determining both the tractive limits of a vehicle, and its behavior below and up to those limits. Figure 8 below shows an example of an MMD plot.

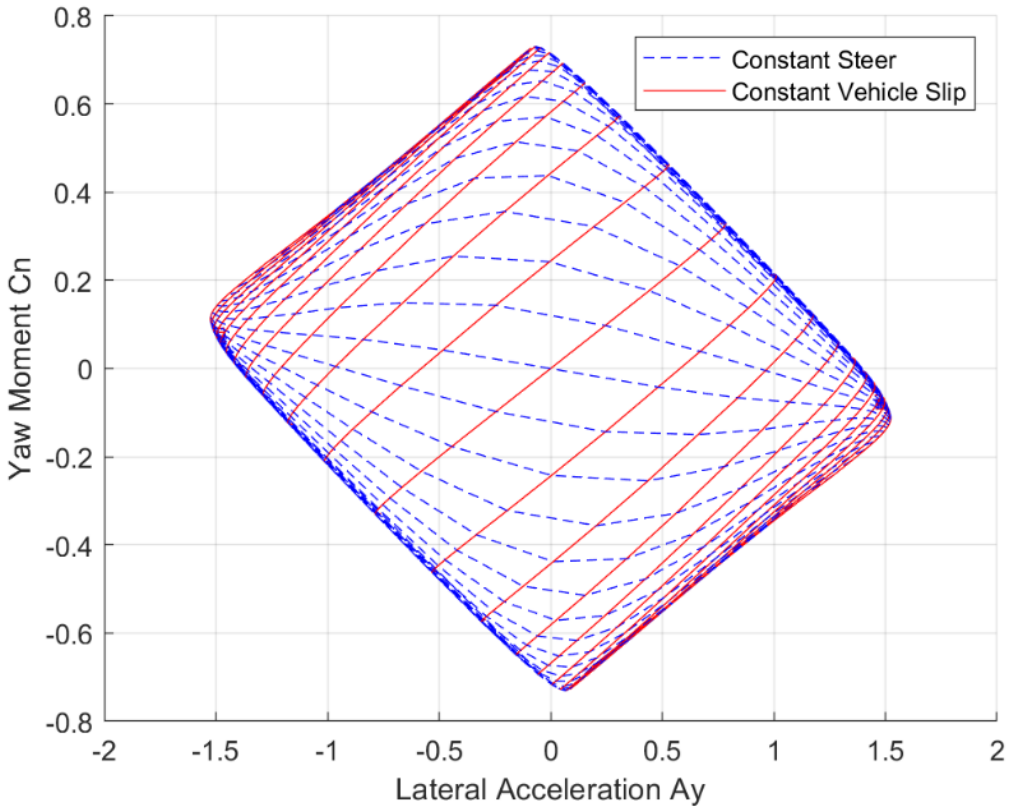

Figure 8: Example of Milliken Moment Diagram – Free Rolling @ 30mph

The plot is created such that lateral acceleration is on the X-axis, and yaw moment coefficient (CN) is on the Y-axis. The blue lines that make up the MMD illustrate the vehicle's behavior when steering angle is held constant, and the red lines are when the vehicle slip angle is held constant. The "edges" that are formed diagonally represent the saturations where the tires are no longer capable of increasing grip when adding additional slip or steering. The right side of the diagram represents right-hand cornering, and the left side represents left-hand cornering. The zero point represents rolling straight ahead at a constant speed with no cornering input. For a symmetric vehicle, the MMD is diagonally symmetric, such that the saturation of the front tires on right-hand corners is represented by the top right edge, and on left-hand corners is represented by the bottom left edge. Similarly, the saturation of the rear tires is represented by the bottom right edge under right-hand cornering, and the top left edge under left-hand cornering.

In addition, there are many other nuances of vehicle behavior that can be retrieved by studying the shapes that comprise the MMD. Vehicle stability at the cornering limit can also be gathered from the MMD by observing where the outer edges cross the X-axis. For example, if the rightmost node is below the X-axis, the vehicle will favor understeer at the limit, and will favor oversteer at the limit if above the X-axis. If the node is closer to the X-axis, the more neutral it will behave at the limit.

Prior to establishing the MMD, the vehicle constants and tire models are determined. Ranges of vehicle slip angles (β) and steering angles (δ) are

selected, along with a constant vehicle speed. The process of creating the MMD involves iterative solving for a given steering angle and vehicle slip angle.

There are a few initialization steps prior to each iteration. By substituting the current vehicle slip angle, the coordinates of each tire can be converted from body-frame to velocity-frame using equations [3] and [4] below.

$$X_i^v = X_i^b \cos\beta + Y_i^b \sin\beta \quad [3]$$

$$Y_i^v = Y_i^b \cos\beta - X_i^b \sin\beta \quad [4]$$

In addition, the initial normal force estimate is set up to assume no weight transfer. Thus, the normal force on each wheel is determined solely by the static weight distribution and downforce loads. Initially, the lateral acceleration and yaw rate (ω) are also set to zero.

In the iteration loop, the tire slip angles are the first to be calculated, which combines yaw rate and vehicle slip. For the first iteration, only the vehicle slip may be nonzero, but resultant yaw rates will be accounted for in subsequent iterations. Equation [5] below is how the individual wheel slip angles are calculated, and equation [6] is the calculation of tire slip angle, accounting for steering angle. Since the vehicle steers with the front wheels, equation [6] is only applied to the front, as the δ of the rear wheels is fixed at zero.

$$\beta_i = \tan^{-1}\frac{V_x \sin\beta + \omega X_i^v}{V_x \cos\beta - \omega Y_i^v} \quad [5]$$

$$\alpha_i = \beta_i - \delta_i \quad [6]$$

Once the individual tire slip angles are determined, all the necessary information can be input into the tire model to get free-rolling forces and moments for each individual corner, assuming no longitudinal slip from driving or braking torque.

When driving or braking torque is applied, an extra level of complexity is added to each iteration. The longitudinal input into the tire model is longitudinal slip, which cannot be accurately estimated by any simple equation. Fortunately, the tire model can be utilized in an unconventional way to back-calculate longitudinal slip from motor torque. The model outputs Fx (longitudinal force) at the tire contact patch, which equates to the wheel torque divided by the rolling radius of the tire. For every wheel in each iteration, Fz, Vx, α, and γ can be held constant. Therefore, it is possible to calculate an array of output Fx values by only varying κ. The outputs are then saved to an array and a linear interpolation is applied to estimate how much slip the individual tire would be subject to.

Figure 9 below is an example of a longitudinal force plot generated by this method. The blue dots are the FX outputs for each κ, and they are linearly interpolated with the blue lines connecting them. The red marker indicates .018 (1.8%) slip will occur when 210N-m of drive torque is applied under these conditions. That equates to 820N of FX. It should be mentioned that this may not be correct after a certain threshold of tire slip past the peak of the tire, which in this case are circled in blue nearby +-0.15 slip. It should only be possible to achieve this threshold under very low-speed maneuvers. This is because the amount of torque required to achieve a given longitudinal slip increases with the vehicle speed.

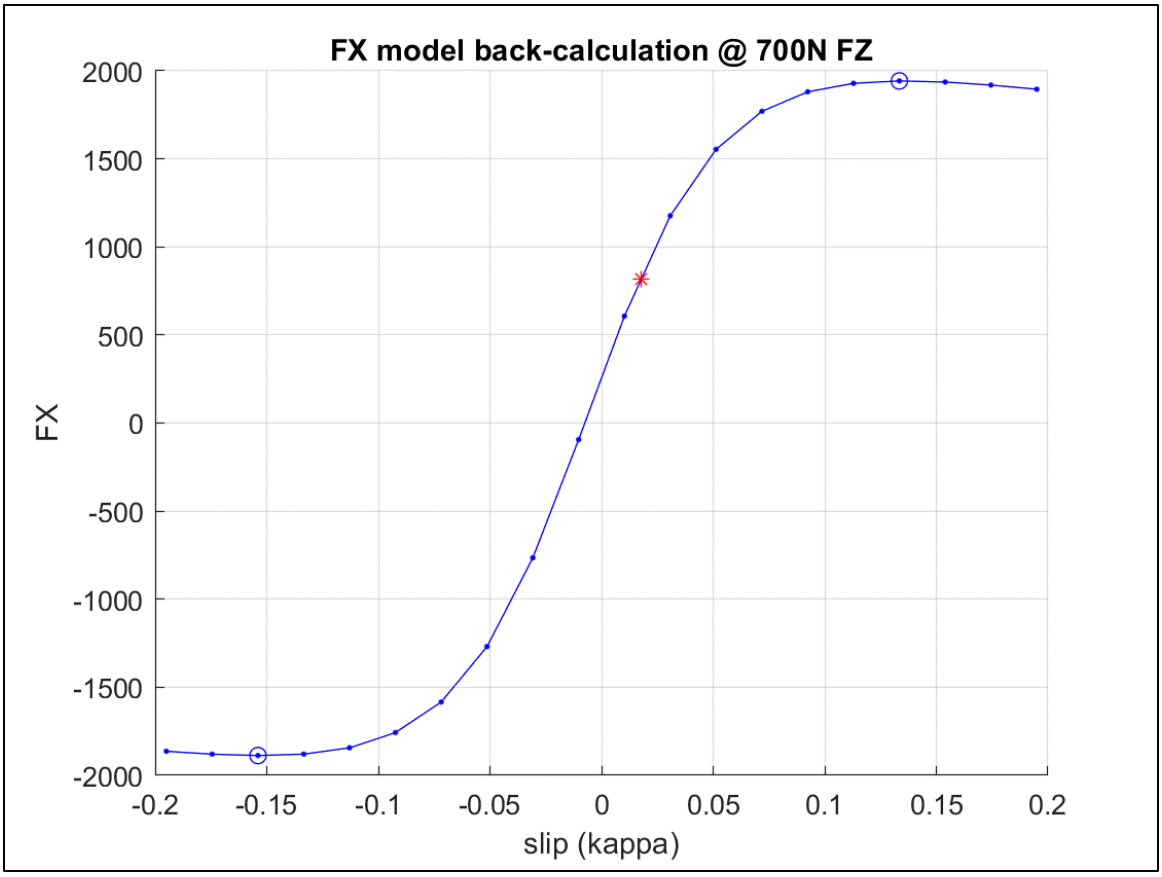

Figure 9: Back-calculation and interpolation of tire model to get longitudinal slip from FX

Once the input conditions are determined, the forces and moments of each tire can be output by the tire model. Then, the resultant forces and moments in the body frame can be calculated by setting up equations of equilibrium [7], [8], and [9] below.

$$F_x = \sum_{i=1}^{4} \left(F_{xi} \cos \delta_i - F_{yi} \sin \delta_i \right) \quad [7]$$

$$F_y = \sum_{i=1}^{4} \left(F_{xi} \sin \delta_i + F_{yi} \cos \delta_i \right) \quad [8]$$

$$M_z = \sum_{i=1}^{4} \left(X_i F_{xi} \sin \delta_i - Y_i F_{xi} \cos \delta_i + Y_i F_{yi} \sin \delta_i + X_i F_{yi} \cos \delta_i \right) \quad [9]$$

With the resultant forces and moments calculated, it is now possible to calculate the accelerations of the vehicle. The lateral acceleration Ay is used as convergence criteria in the iteration. Ay is also plotted in the MMD along with yaw moment coefficient Cn. Equations [10], [11], and [12] below are used to calculate longitudinal and lateral accelerations, as well as yaw moment coefficient.

$$A_x = \frac{F_x}{mg} = \frac{F_x}{W} \quad [10]$$

$$A_y = \frac{F_y}{mg} = \frac{F_y}{W} \quad [11]$$

$$C_n = \frac{M_z}{mgL} = \frac{M_z}{WL} \quad [12]$$

By substituting the lateral and longitudinal accelerations, the yaw rate and updated loads can be calculated. All of these are then saved and substituted into the equations, starting the next iteration. Equations [13] and [14] below are used to calculate yaw rate ω.

$$\omega_{est} = \frac{A_y}{V_x} \quad [13]$$

$$\omega = \omega_{est}(1 - p_r) + \omega_{old} * p_r \quad [14]$$

Equation [14] is an updated ω which is “relaxed” to a value between the original ω and recalculated ω, determined by the relaxation constant Pr. This is to avoid the recalculated ω from overshooting the correct value, which has the potential to cause convergence errors [10].

Equations [15] through [18] are the equations which calculate normal force on each of the tires based on the accelerations. Due to the behavior of weight transfer, the weight will shift away from the direction the vehicle is accelerating.

$$F_{z,fl} = \max\left(\frac{W_f}{2} + \frac{dF_{zf}}{dA_{xb}}Ax + \frac{dF_{zf}}{dA_{yb}}Ay + \frac{DF_f}{2}, 0.1\right) \quad [15]$$

$$F_{z,fr} = \max\left(\frac{W_f}{2} + \frac{dF_{zf}}{dA_{xb}}Ax - \frac{dF_{zf}}{dA_{yb}}Ay + \frac{DF_f}{2}, 0.1\right) \quad [16]$$

$$F_{z,rl} = \max\left(\frac{W_r}{2} - \frac{dF_{zf}}{dA_{xb}}Ax + \frac{dF_{zf}}{dA_{yb}}Ay + \frac{DF_r}{2}, 0.1\right) \quad [17]$$

$$F_{z,rr} = \max\left(\frac{W_r}{2} - \frac{dF_{zf}}{dA_{xb}}Ax - \frac{dF_{zf}}{dA_{yb}}Ay + \frac{DF_r}{2}, 0.1\right) \quad [18]$$

Something to consider is that at high lateral accelerations, the weight transferred off a tire may outweigh the static normal force on the tire in the first place. In practice, this behavior would cause the tire to lift off the ground. A

rudimentary “max” function was implemented above to avoid this phenomenon which would cause an incorrect negative normal force on a corner. This is not a perfect solution, and the transition still causes some anomalies in the MMD, as shown on Figure 10 below at +-2.4G of Ay.

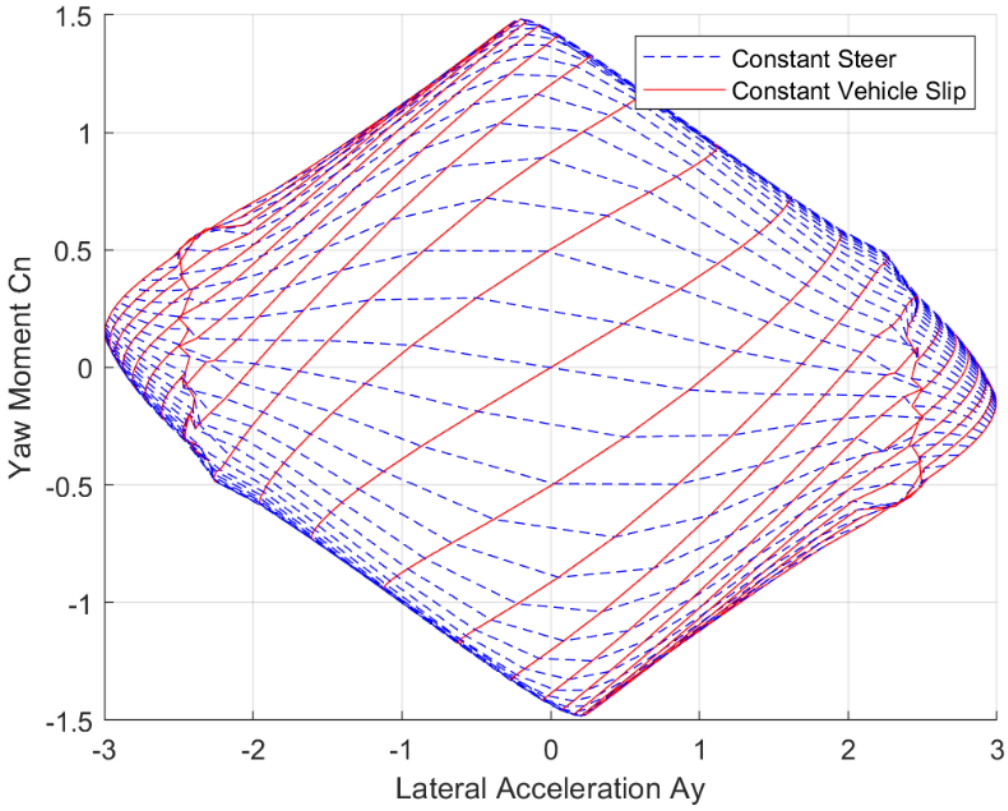

Figure 10: Free Rolling MMD output plot

The disruptions are not critical to the simulation, since the focus is on peak yaw moment rather than peak lateral acceleration, which is when this phenomenon occurs. However, refining the vehicle suspension model should be able to alleviate this issue if required for future development.

At this point, the convergence will be checked as everything has been calculated for the specific conditions in the MMD. The criterion for convergence is that the newly calculated Ay is within 0.1% of the value from the previous iteration. The loop will proceed with the new loads, accelerations, and yaw rate if the criteria is not met. Figure 11 below shows the flowchart for the iterative method used.

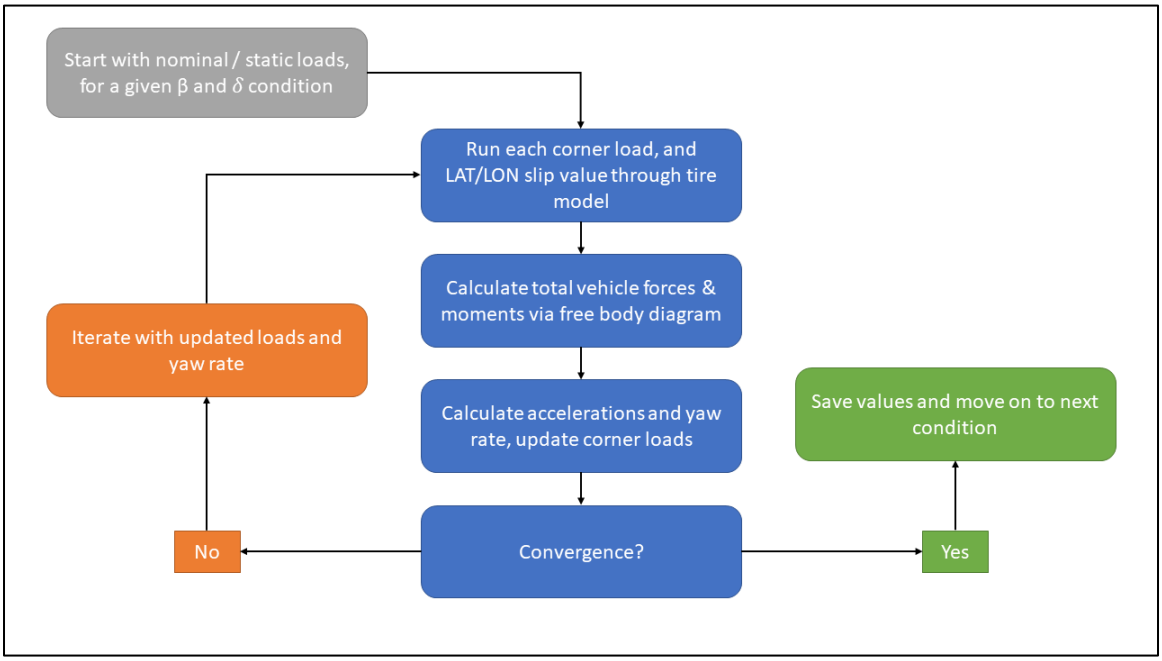

Figure 11: Flowchart of MMD Generation Process

CHAPTER V

SIMULATION AND MMD RESULTS

The first MMD completed was performed on a vehicle in a “free rolling” state, without driving or braking torque applied to any of the wheels. Since no torque was applied, this can be considered the simulation for motor configuration (i). The resultant diagram from the free rolling vehicle simulation can be found on Figure 10 in Chapter IV. The peak yaw coefficient achieved by this setup is 1.48, and the peak lateral acceleration falls just under 3.0G at 2.99.

The next MMD’s to be constructed were those of the rear-wheel-drive configurations. These were still simulated without any drive or brake input, but the individual motor torques are augmented using the scaling factor from Chapter I. Figures 12 and 13 below show the resultant MMD’s of configurations without (ii) and with inside regen (iii), respectively. There is a visible improvement in overall yaw capability, while lateral acceleration stays the same at 2.99. Configuration (ii) has marginally higher peak Cn at 1.56, while Cn in (iii) saw much higher improvements of its peak to 1.68. These results illustrate that applying negative torque to the inside wheels makes a more significant improvement than solely increasing torque to the outside. Also, observing the rightmost point of the MMD shows that with inside regen, the vehicle becomes slightly more stable and less prone to understeer.

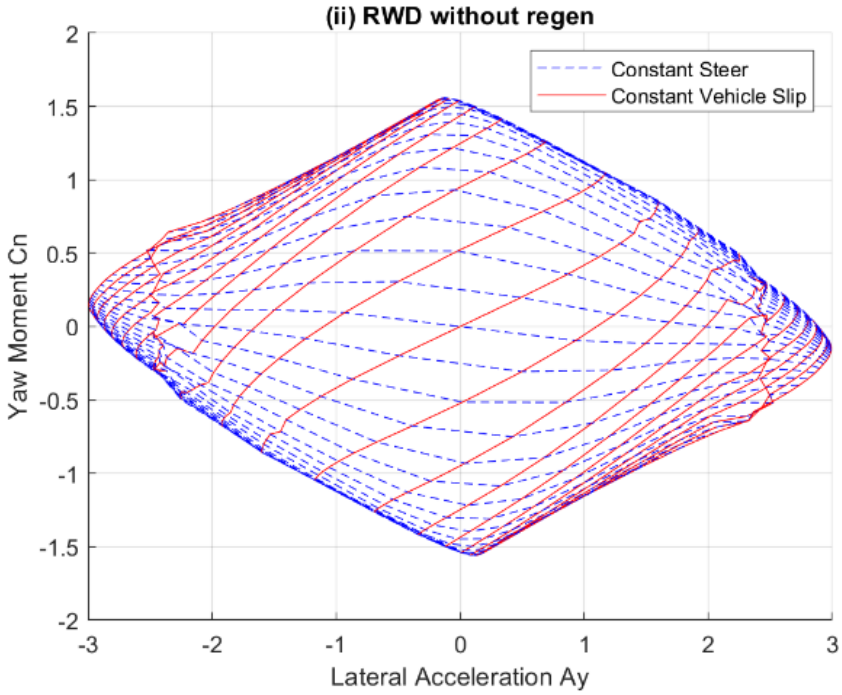

Figure 12: MMD plot of RWD TV configuration (ii) without inside wheel regeneration

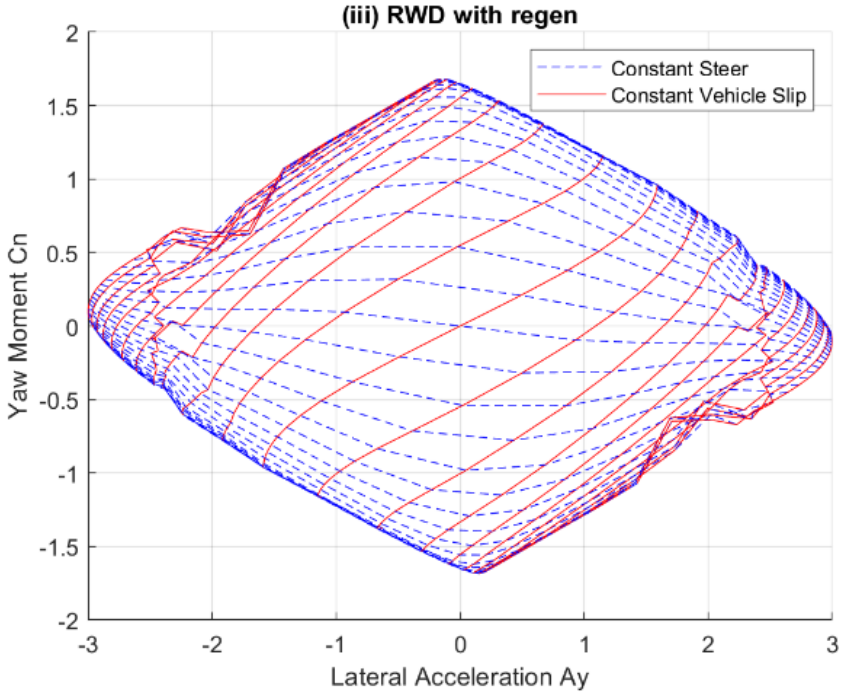

Figure 13: MMD plot of RWD TV configuration (iii) with inside wheel regeneration

The other two configurations to be simulated were with TV on all 4 wheels, without (iv) and with inside regen (v). Figures 14 and 15 below show the MMD results of these configurations. The trends found in the RWD configurations also apply here to the AWD configurations, but on a greater scale. Predictably, Configuration (v) has the highest peak Cn, which equates to 1.87. In addition, configuration (iv) also output a noticeable increase in peak Cn, at 1.70. Both configurations still show a max Ay of 2.99G. Also, similarly to the RWD configurations, the example with regen will behave more neutrally, while it will understeer slightly without regen.

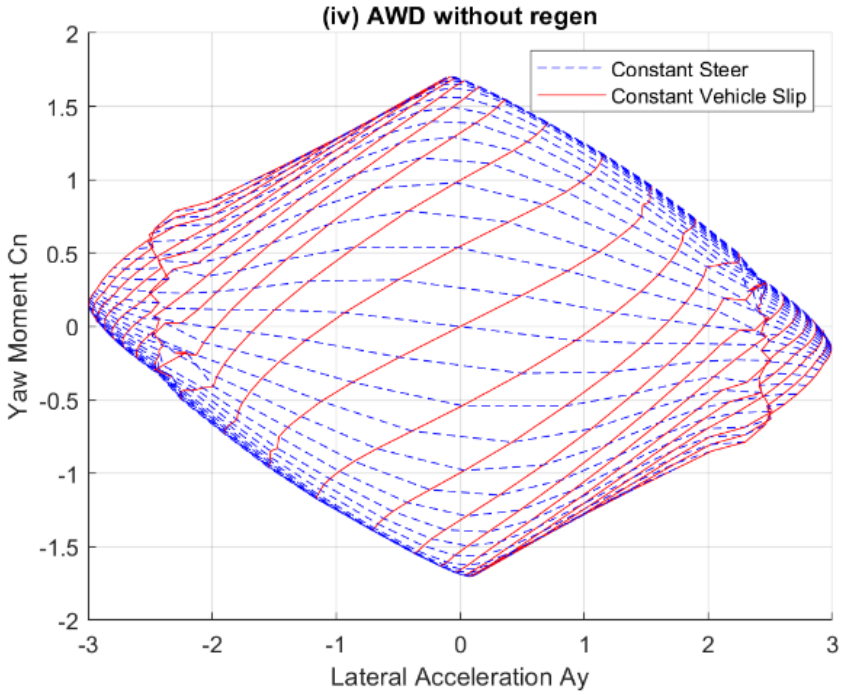

Figure 14: MMD plot of AWD TV configurations (iv) without inside wheel regeneration

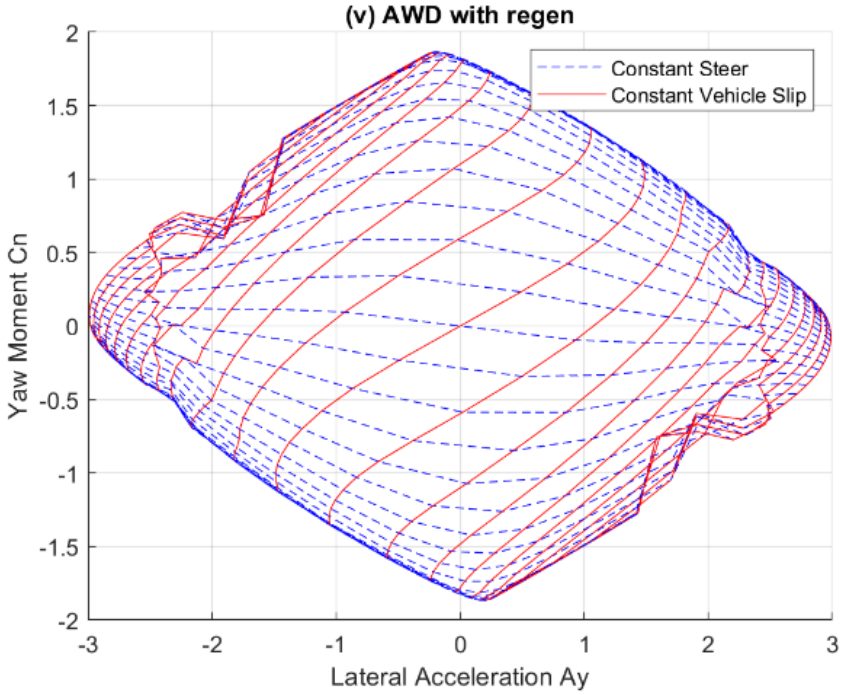

Figure 15: MMD plot of AWD TV configuration (v) with inside wheel regeneration

For each motor contributing to TV, the ability of the vehicle to yaw increases by approximately 0.097 Cn. In perspective, each motor contributing to TV increases the vehicle's yaw capability by 6.5% up to a maximum of 26.4% of its original capability. To visually compare between all configurations, steering angle sweeps were overlaid for constant vehicle slip angles of 0 and 3 degrees in Figures 16 and 17 below, respectively. These plots help confirm the trends seen in all the MMDs.

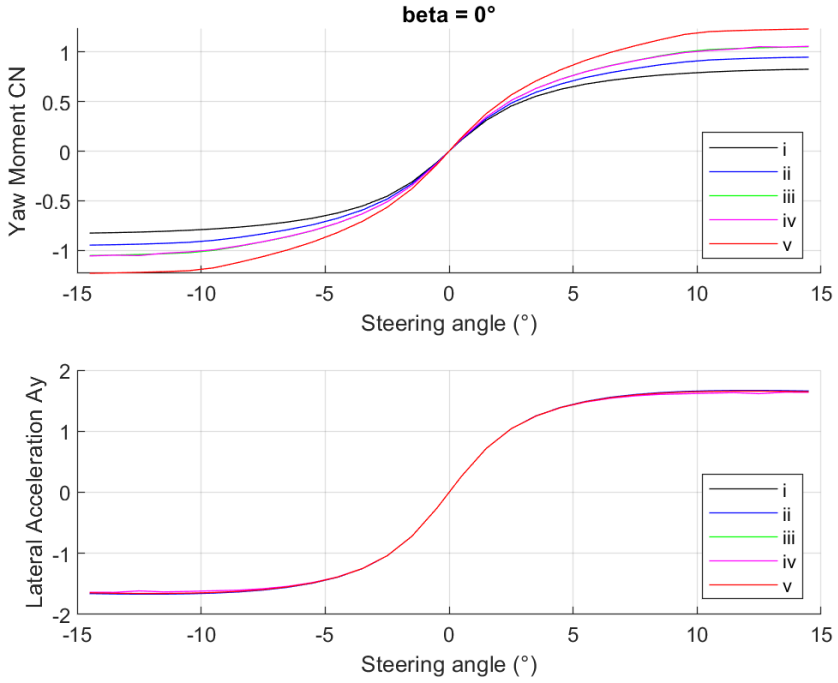

Figure 16: Steering Angle Sweeps in MMD of 0° vehicle slip

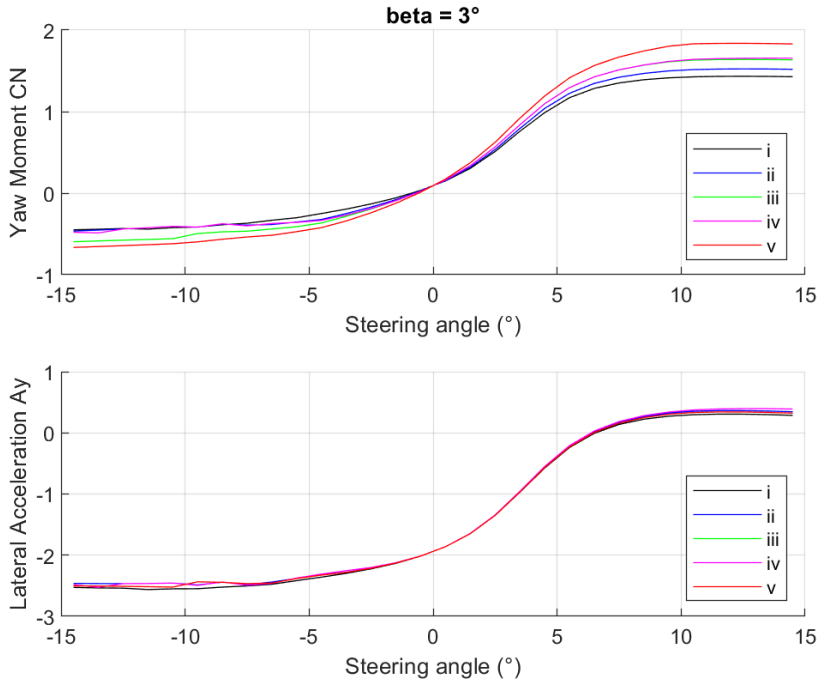

Figure 17: Steering Angle Sweeps in MMD of 3° vehicle slip

While these sweeps scale similarly to the MMDs, an interesting comparison can be found between configurations (iii) and (iv). Both have two motors contributing to torque vectoring, however, they both have comparable yaw capabilities. In fact, while an AWD TV system like (iv) without regen will have marginally higher Cn than a RWD TV system with regen like (iii), the RWD system is dynamically more neutral than the AWD, plus has the advantages of being a lighter and simpler system. That said, the AWD system will have traction advantages outside of steady-state cornering, but a RWD TV system can be dynamically almost as effective as an AWD TV system if constraints do not allow an AWD powertrain.

CHAPTER VI

VARIATION OF INPUTS AND TORQUE CONTROL MAP

To verify robustness, conditions were varied and compared in the model. The first condition to be varied was speed. The hypothesis is that TV will be more effective at lower-speed cornering maneuvers, such as hairpins. To achieve the same longitudinal slip in the tires, less torque is necessary to achieve the same slip at lower speed due to how slip is calculated, in addition to less downforce.

Figures 18 and 19 below show the MMDs of configurations (i) and (v), respectively, when they underwent speeds of 20, 30, and 40mph. It can be observed that peak Ay stays the same regardless of speed. At 20mph, Cn improves from 1.38 to 1.76, which is a 27.5% improvement. At 40mph, Cn improves from 1.62 to 2.01, improving by 24.1%. Referencing Figures 10 and 14, the improvement seen at 30mph is 26.4%, thus there is an improvement to the yaw contribution of TV when speed is reduced. This becomes especially important when factoring in the tight and technical autocross courses commonplace in FSAE competitions.

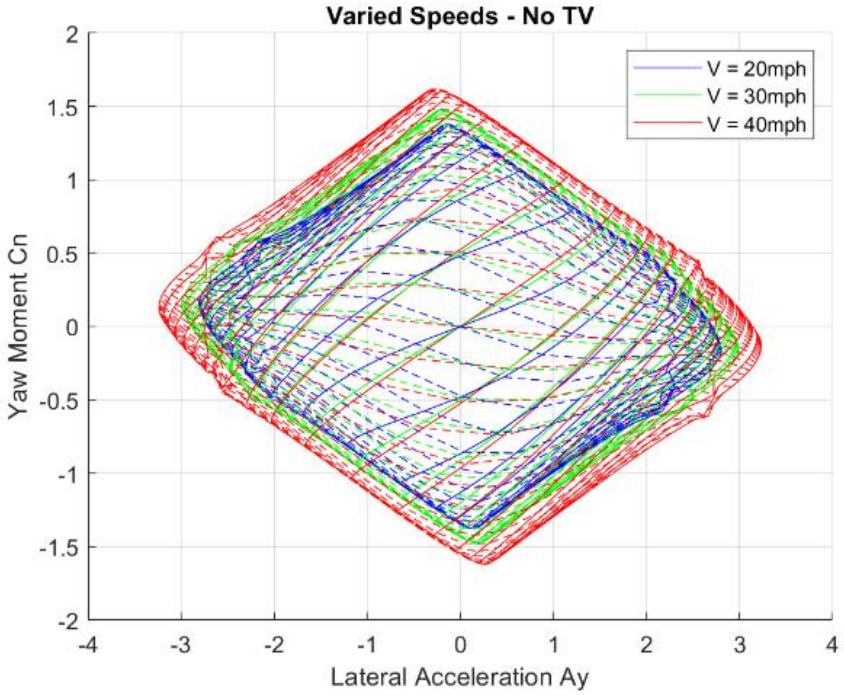

Figure 18: Overlaid MMDs at various speeds of configuration (i)

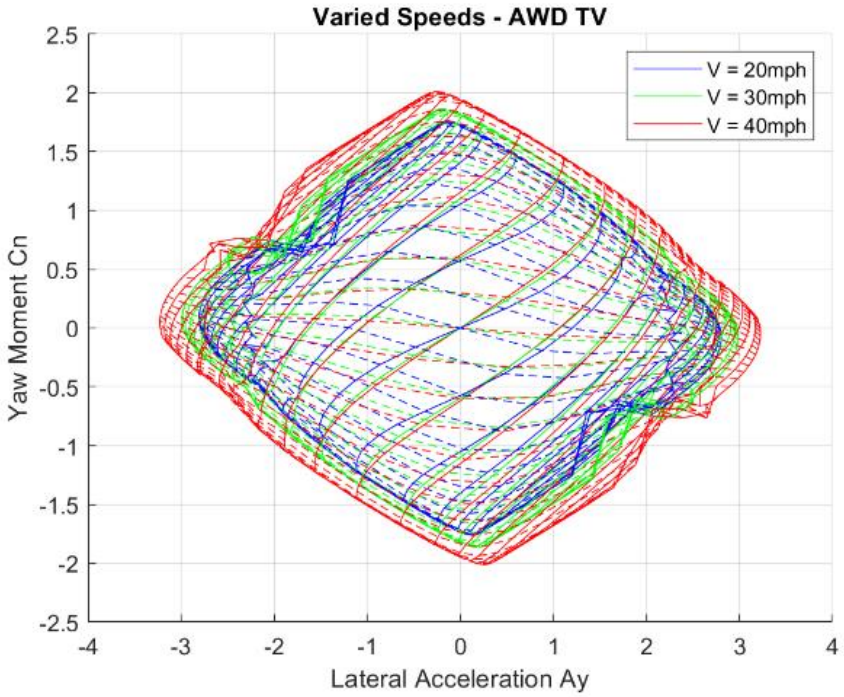

Figure 19: Overlaid MMDs at various speeds of configuration (v)

Next, front/rear motor torque bias was varied in the simulation to observe the effects in cornering. This is the proportion of total torque applied to either the front or rear axle, which is similar in concept to brake bias on a conventional racing car. While the maximum torque output is not modified, this changes how torque is distributed from front to rear up to when the motors reach their peak torque.

Figure 20 below shows the resultant MMD's overlaid from varying this torque bias. There is only a minute difference, so the peak positive Cn was zoomed in for detail on Figure 21 below. The peak Cn of the 50% and 70% rearward biased examples are notably identical at 1.87, however they slightly differ elsewhere inside the diagram. This portion of the code can be used to optimize front/rear motor bias, particularly when throttle is applied upon corner exit to optimize both longitudinal and lateral acceleration, in addition to yaw.

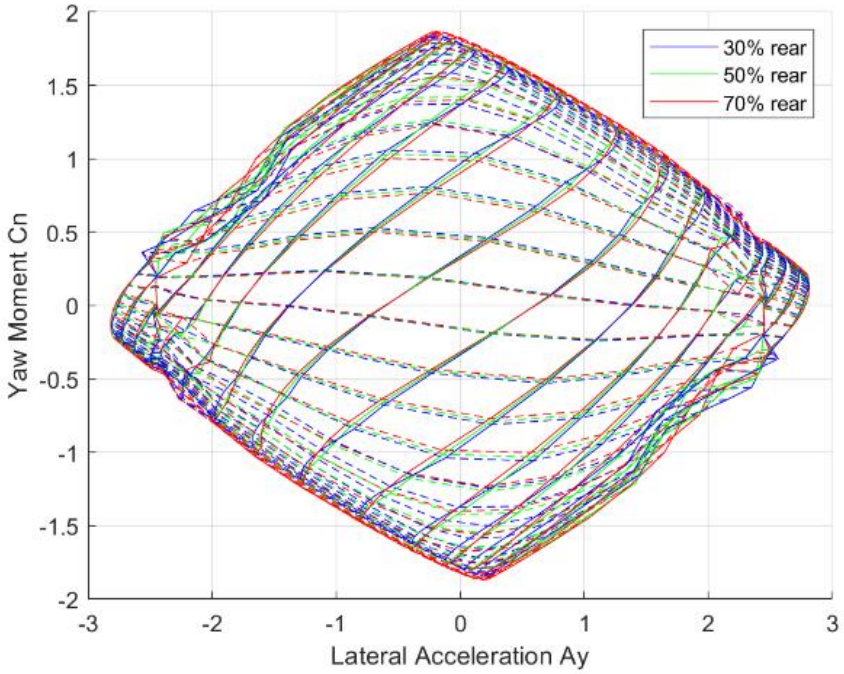

Figure 20: MMD comparison when front/rear torque bias is varied

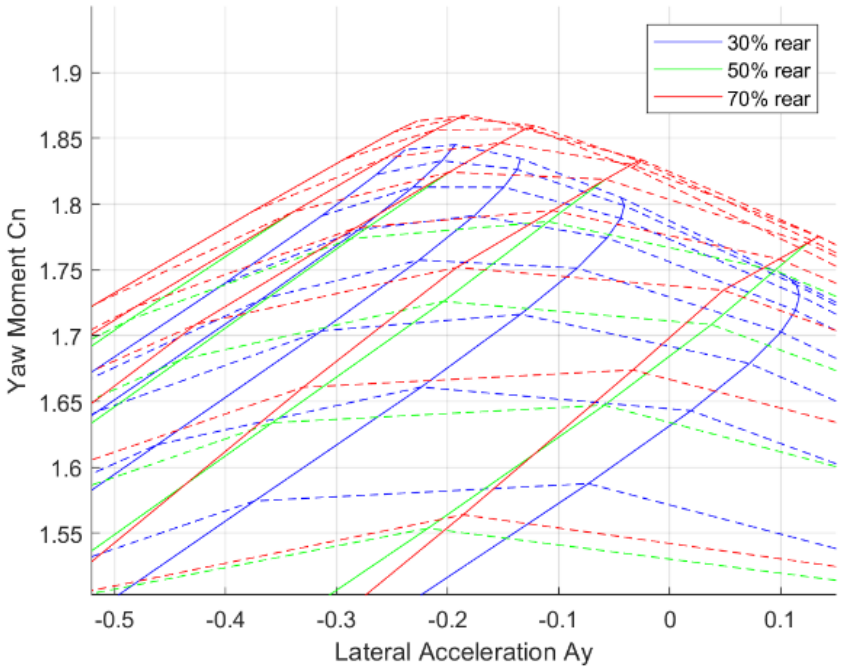

Figure 21: Detail view of peak yaw moment comparison from Figure 20

Another condition to be varied is the longitudinal acceleration and deceleration. Up to this point, the vehicle has not exhibited any resultant acceleration longitudinally, as the motor torques were always opposing each other in this direction during TV. Prior to simulating this portion, it made sense to construct a detailed “map” of the motor outputs from a given steering and throttle input. This map applies the torque vectoring scalar of 21Nm/° of steering angle, while also taking account of the limitations of peak motor torque, and maximum total power output by the FSAE regulations.

To achieve this map, another scalar was created to factor motor output versus throttle position. Simultaneously, a “neutral” throttle position was set to 15% of pedal travel, which determines when the resultant motor torques amount to zero. When the vehicle is in motion, throttle input below this neutral position would result in regenerative torque being applied, which would provide a similar sensation to parasitic losses in a combustion engine powered vehicle. This means that the MMD’s simulated above all correspond to 15% throttle in this instance. The motor output scalar was subsequently created by linearly interpolating the neutral data point with the maximum 210 Nm of every motor at 100% throttle. This resulted in a factor of 2.47Nm of torque from each motor per one percent increase of throttle.

Tables 1 and 2 below show the output of the created maps for each side of the vehicle. Since 50% front/rear motor torque bias is being used, each front motor has identical torque commands as the corresponding rear motor of the same side. Due to the symmetry of the setup, the left-hand table is a mirror

image of the right-hand table about the neutral steering axis. The variables considered on these maps are steering angle (x-axis) and throttle position (y-axis). Each of the successive tables have a standardized output format to make them easier to visualize. The stronger shades of blue indicate more positive torque being applied to each motor, and the stronger shades of red indicate more negative torque, while white is zero torque.

Table 1: Right-hand side motor commanded torque map

FR
RR

TPS (%) \ steering angle (deg)	-15	-14	-13	-12	-11	-10	-9	-8	-7	-6	-5	-4	-3	-2	-1	0	1	2	3	4	5	6	7	8	9	10	11	12	13	14	15
0	-210.0	-210.0	-210.0	-210.0	-210.0	-210.0	-210.0	-205.1	-184.1	-163.1	-142.1	-121.1	-100.1	-79.1	-58.1	-37.1	-16.1	4.9	25.9	46.9	67.9	88.9	109.9	130.9	151.9	172.9	193.9	210.0	210.0	210.0	210.0
5	-210.0	-210.0	-210.0	-210.0	-210.0	-210.0	-210.0	-192.7	-171.7	-150.7	-129.7	-108.7	-87.7	-66.7	-45.7	-24.7	-3.7	17.3	38.3	59.3	80.3	101.3	122.3	143.3	164.3	185.3	206.3	210.0	210.0	210.0	210.0
10	-210.0	-210.0	-210.0	-210.0	-210.0	-210.0	-201.4	-180.4	-159.4	-138.4	-117.4	-96.4	-75.4	-54.4	-33.4	-12.4	8.6	29.6	50.6	71.6	92.6	113.6	134.6	155.6	176.6	197.6	210.0	210.0	210.0	210.0	210.0
15	-210.0	-210.0	-210.0	-210.0	-210.0	-210.0	-189.0	-168.0	-147.0	-126.0	-105.0	-84.0	-63.0	-42.0	-21.0	0.0	21.0	42.0	63.0	84.0	105.0	126.0	147.0	168.0	189.0	210.0	210.0	210.0	210.0	210.0	210.0
20	-210.0	-210.0	-210.0	-210.0	-210.0	-197.6	-176.6	-155.6	-134.6	-113.6	-92.6	-71.6	-50.6	-29.6	-8.6	12.4	33.4	54.4	75.4	96.4	117.4	138.4	159.4	180.4	201.4	210.0	210.0	210.0	210.0	210.0	210.0
25	-210.0	-210.0	-210.0	-210.0	-206.3	-185.3	-164.3	-143.3	-122.3	-101.3	-80.3	-59.3	-38.3	-17.3	3.7	24.7	45.7	66.7	87.7	108.7	129.7	150.7	171.7	192.7	210.0	210.0	210.0	210.0	210.0	210.0	210.0
30	-210.0	-210.0	-210.0	-210.0	-193.9	-172.9	-151.9	-130.9	-109.9	-88.9	-67.9	-46.9	-25.9	-4.9	16.1	37.1	58.1	79.1	100.1	121.1	142.1	163.1	184.1	205.1	210.0	210.0	210.0	210.0	210.0	210.0	210.0
35	-210.0	-210.0	-210.0	-202.6	-181.6	-160.6	-139.6	-118.6	-97.6	-76.6	-55.6	-34.6	-13.6	7.4	28.4	49.4	70.4	91.4	112.4	133.4	154.4	175.4	196.4	210.0	210.0	210.0	210.0	210.0	210.0	210.0	210.0
40	-210.0	-210.0	-210.0	-190.2	-169.2	-148.2	-127.2	-106.2	-85.2	-64.2	-43.2	-22.2	-1.2	19.8	40.8	61.8	82.8	103.8	124.8	145.8	166.8	187.8	208.8	210.0	210.0	210.0	210.0	210.0	210.0	210.0	210.0
45	-210.0	-210.0	-198.9	-177.9	-156.9	-135.9	-114.9	-93.9	-72.9	-51.9	-30.9	-9.9	11.1	32.1	53.1	74.1	95.1	116.1	137.1	158.1	179.1	200.1	210.0	210.0	210.0	210.0	210.0	210.0	210.0	210.0	210.0
50	-210.0	-207.5	-186.5	-165.5	-144.5	-123.5	-102.5	-81.5	-60.5	-39.5	-18.5	2.5	23.5	44.5	65.5	86.5	107.5	128.5	149.5	170.5	191.5	210.0	210.0	210.0	210.0	210.0	210.0	210.0	210.0	210.0	210.0
55	-210.0	-195.2	-174.2	-153.2	-132.2	-111.2	-90.2	-69.2	-48.2	-27.2	-6.2	14.8	35.8	56.8	77.8	98.8	119.8	140.8	161.8	182.8	203.8	210.0	210.0	210.0	210.0	210.0	210.0	210.0	210.0	210.0	210.0
60	-203.8	-182.8	-161.8	-140.8	-119.8	-98.8	-77.8	-56.8	-35.8	-14.8	6.2	27.2	48.2	69.2	90.2	111.2	132.2	153.2	174.2	195.2	210.0	210.0	210.0	210.0	210.0	210.0	210.0	210.0	210.0	210.0	210.0
65	-191.5	-170.5	-149.5	-128.5	-107.5	-86.5	-65.5	-44.5	-23.5	-2.5	18.5	39.5	60.5	81.5	102.5	123.5	144.5	165.5	186.5	207.5	210.0	210.0	210.0	210.0	210.0	210.0	210.0	210.0	210.0	210.0	210.0
70	-179.1	-158.1	-137.1	-116.1	-95.1	-74.1	-53.1	-32.1	-11.1	9.9	30.9	51.9	72.9	93.9	114.9	135.9	156.9	177.9	198.9	210.0	210.0	210.0	210.0	210.0	210.0	210.0	210.0	210.0	210.0	210.0	210.0
75	-166.8	-145.8	-124.8	-103.8	-82.8	-61.8	-40.8	-19.8	1.2	22.2	43.2	64.2	85.2	106.2	127.2	148.2	169.2	190.2	210.0	210.0	210.0	210.0	210.0	210.0	210.0	210.0	210.0	210.0	210.0	210.0	210.0
80	-154.4	-133.4	-112.4	-91.4	-70.4	-49.4	-28.4	-7.4	13.6	34.6	55.6	76.6	97.6	118.6	139.6	160.6	181.6	202.6	210.0	210.0	210.0	210.0	210.0	210.0	210.0	210.0	210.0	210.0	210.0	210.0	210.0
85	-142.1	-121.1	-100.1	-79.1	-58.1	-37.1	-16.1	4.9	25.9	46.9	67.9	88.9	109.9	130.9	151.9	172.9	193.9	210.0	210.0	210.0	210.0	210.0	210.0	210.0	210.0	210.0	210.0	210.0	210.0	210.0	210.0
90	-129.7	-108.7	-87.7	-66.7	-45.7	-24.7	-3.7	17.3	38.3	59.3	80.3	101.3	122.3	143.3	164.3	185.3	206.3	210.0	210.0	210.0	210.0	210.0	210.0	210.0	210.0	210.0	210.0	210.0	210.0	210.0	210.0
95	-117.4	-96.4	-75.4	-54.4	-33.4	-12.4	8.6	29.6	50.6	71.6	92.6	113.6	134.6	155.6	176.6	197.6	210.0	210.0	210.0	210.0	210.0	210.0	210.0	210.0	210.0	210.0	210.0	210.0	210.0	210.0	210.0
100	-105.0	-84.0	-63.0	-42.0	-21.0	0.0	21.0	42.0	63.0	84.0	105.0	126.0	147.0	168.0	189.0	210.0	210.0	210.0	210.0	210.0	210.0	210.0	210.0	210.0	210.0	210.0	210.0	210.0	210.0	210.0	210.0

Table 2: Left-hand side motor commanded torque map

FL
RL

TPS (%) \ steering angle (deg)	-15	-14	-13	-12	-11	-10	-9	-8	-7	-6	-5	-4	-3	-2	-1	0	1	2	3	4	5	6	7	8	9	10	11	12	13	14	15
0	210.0	210.0	210.0	210.0	193.9	172.9	151.9	130.9	109.9	88.9	67.9	46.9	25.9	4.9	-16.1	-37.1	-58.1	-79.1	-100.1	-121.1	-142.1	-163.1	-184.1	-205.1	-210.0	-210.0	-210.0	-210.0	-210.0	-210.0	-210.0
5	210.0	210.0	210.0	210.0	206.3	185.3	164.3	143.3	122.3	101.3	80.3	59.3	38.3	17.3	-3.7	-24.7	-45.7	-66.7	-87.7	-108.7	-129.7	-150.7	-171.7	-192.7	-210.0	-210.0	-210.0	-210.0	-210.0	-210.0	-210.0
10	210.0	210.0	210.0	210.0	210.0	197.6	176.6	155.6	134.6	113.6	92.6	71.6	50.6	29.6	8.6	-12.4	-33.4	-54.4	-75.4	-96.4	-117.4	-138.4	-159.4	-180.4	-201.4	-210.0	-210.0	-210.0	-210.0	-210.0	-210.0
15	210.0	210.0	210.0	210.0	210.0	210.0	189.0	168.0	147.0	126.0	105.0	84.0	63.0	42.0	21.0	0.0	-21.0	-42.0	-63.0	-84.0	-105.0	-126.0	-147.0	-168.0	-189.0	-210.0	-210.0	-210.0	-210.0	-210.0	-210.0
20	210.0	210.0	210.0	210.0	210.0	210.0	201.4	180.4	159.4	138.4	117.4	96.4	75.4	54.4	33.4	12.4	-8.6	-29.6	-50.6	-71.6	-92.6	-113.6	-134.6	-155.6	-176.6	-197.6	-210.0	-210.0	-210.0	-210.0	-210.0
25	210.0	210.0	210.0	210.0	210.0	210.0	210.0	192.7	171.7	150.7	129.7	108.7	87.7	66.7	45.7	24.7	3.7	-17.3	-38.3	-59.3	-80.3	-101.3	-122.3	-143.3	-164.3	-185.3	-206.3	-210.0	-210.0	-210.0	-210.0
30	210.0	210.0	210.0	210.0	210.0	210.0	210.0	205.1	184.1	163.1	142.1	121.1	100.1	79.1	58.1	37.1	16.1	-4.9	-25.9	-46.9	-67.9	-88.9	-109.9	-130.9	-151.9	-172.9	-193.9	-210.0	-210.0	-210.0	-210.0
35	210.0	210.0	210.0	210.0	210.0	210.0	210.0	210.0	196.4	175.4	154.4	133.4	112.4	91.4	70.4	49.4	28.4	7.4	-13.6	-34.6	-55.6	-76.6	-97.6	-118.6	-139.6	-160.6	-181.6	-202.6	-210.0	-210.0	-210.0
40	210.0	210.0	210.0	210.0	210.0	210.0	210.0	210.0	208.8	187.8	166.8	145.8	124.8	103.8	82.8	61.8	40.8	19.8	-1.2	-22.2	-43.2	-64.2	-85.2	-106.2	-127.2	-148.2	-169.2	-190.2	-210.0	-210.0	-210.0
45	210.0	210.0	210.0	210.0	210.0	210.0	210.0	210.0	210.0	200.1	179.1	158.1	137.1	116.1	95.1	74.1	53.1	32.1	11.1	-9.9	-30.9	-51.9	-72.9	-93.9	-114.9	-135.9	-156.9	-177.9	-198.9	-210.0	-210.0
50	210.0	210.0	210.0	210.0	210.0	210.0	210.0	210.0	210.0	210.0	191.5	170.5	149.5	128.5	107.5	86.5	65.5	44.5	23.5	2.5	-18.5	-39.5	-60.5	-81.5	-102.5	-123.5	-144.5	-165.5	-186.5	-207.5	-210.0
55	210.0	210.0	210.0	210.0	210.0	210.0	210.0	210.0	210.0	210.0	203.8	182.8	161.8	140.8	119.8	98.8	77.8	56.8	35.8	14.8	-6.2	-27.2	-48.2	-69.2	-90.2	-111.2	-132.2	-153.2	-174.2	-195.2	-210.0
60	210.0	210.0	210.0	210.0	210.0	210.0	210.0	210.0	210.0	210.0	210.0	195.2	174.2	153.2	132.2	111.2	90.2	69.2	48.2	27.2	6.2	-14.8	-35.8	-56.8	-77.8	-98.8	-119.8	-140.8	-161.8	-182.8	-203.8
65	210.0	210.0	210.0	210.0	210.0	210.0	210.0	210.0	210.0	210.0	210.0	207.5	186.5	165.5	144.5	123.5	102.5	81.5	60.5	39.5	18.5	-2.5	-23.5	-44.5	-65.5	-86.5	-107.5	-128.5	-149.5	-170.5	-191.5
70	210.0	210.0	210.0	210.0	210.0	210.0	210.0	210.0	210.0	210.0	210.0	210.0	198.9	177.9	156.9	135.9	114.9	93.9	72.9	51.9	30.9	9.9	-11.1	-32.1	-53.1	-74.1	-95.1	-116.1	-137.1	-158.1	-179.1
75	210.0	210.0	210.0	210.0	210.0	210.0	210.0	210.0	210.0	210.0	210.0	210.0	210.0	190.2	169.2	148.2	127.2	106.2	85.2	64.2	43.2	22.2	1.2	-19.8	-40.8	-61.8	-82.8	-103.8	-124.8	-145.8	-166.8
80	210.0	210.0	210.0	210.0	210.0	210.0	210.0	210.0	210.0	210.0	210.0	210.0	210.0	202.6	181.6	160.6	139.6	118.6	97.6	76.6	55.6	34.6	13.6	-7.4	-28.4	-49.4	-70.4	-91.4	-112.4	-133.4	-154.4
85	210.0	210.0	210.0	210.0	210.0	210.0	210.0	210.0	210.0	210.0	210.0	210.0	210.0	210.0	193.9	172.9	151.9	130.9	109.9	88.9	67.9	46.9	25.9	4.9	-16.1	-37.1	-58.1	-79.1	-100.1	-121.1	-142.1
90	210.0	210.0	210.0	210.0	210.0	210.0	210.0	210.0	210.0	210.0	210.0	210.0	210.0	210.0	206.3	185.3	164.3	143.3	122.3	101.3	80.3	59.3	38.3	17.3	-3.7	-24.7	-45.7	-66.7	-87.7	-108.7	-129.7
95	210.0	210.0	210.0	210.0	210.0	210.0	210.0	210.0	210.0	210.0	210.0	210.0	210.0	210.0	210.0	197.6	176.6	155.6	134.6	113.6	92.6	71.6	50.6	29.6	8.6	-12.4	-33.4	-54.4	-75.4	-96.4	-117.4
100	210.0	210.0	210.0	210.0	210.0	210.0	210.0	210.0	210.0	210.0	210.0	210.0	210.0	210.0	210.0	210.0	189.0	168.0	147.0	126.0	105.0	84.0	63.0	42.0	21.0	0.0	-21.0	-42.0	-63.0	-84.0	-105.0

The total torque at each point in the map can be found by combining the torque values from the same respective point in each map together. In the case of 50% rear bias, the resultant would be two of the same right-hand value, and

two of the same left-hand value. Table 3 below shows the total torque output with the chosen map. Total power output can be calculated for a given vehicle speed by factoring in the tire size and gearbox ratio, which is shown in Table 4 below.

Table 3: Combined map of torque output of all four motors

TOTAL	steering angle (deg)																												
TPS (%)	-15	-14	-13	-12	-11	-10	-9	-8	-7	-6	-5	-4	-3	-2	-1	0	1	2	3	4	5	6	7	8	9	10	11	12	13	14	15
0	0.0	0.0	0.0	0.0	-32.1	-74.1	-116.1	-148.2	-148.2	-148.2	-148.2	-148.2	-148.2	-148.2	-148.2	-148.2	-148.2	-148.2	-148.2	-148.2	-148.2	-148.2	-148.2	-148.2	-116.1	-74.1	-32.1	0.0	0.0	0.0	0.0
5	0.0	0.0	0.0	0.0	-7.4	-49.4	-91.4	-98.8	-98.8	-98.8	-98.8	-98.8	-98.8	-98.8	-98.8	-98.8	-98.8	-98.8	-98.8	-98.8	-98.8	-98.8	-98.8	-98.8	-91.4	-49.4	-7.4	0.0	0.0	0.0	0.0
10	0.0	0.0	0.0	0.0	0.0	-24.7	-49.4	-49.4	-49.4	-49.4	-49.4	-49.4	-49.4	-49.4	-49.4	-49.4	-49.4	-49.4	-49.4	-49.4	-49.4	-49.4	-49.4	-49.4	-49.4	-24.7	0.0	0.0	0.0	0.0	0.0
15	0.0	0.0	0.0	0.0	0.0	0.0	0.0	0.0	0.0	0.0	0.0	0.0	0.0	0.0	0.0	0.0	0.0	0.0	0.0	0.0	0.0	0.0	0.0	0.0	0.0	0.0	0.0	0.0	0.0	0.0	0.0
20	0.0	0.0	0.0	0.0	0.0	24.7	49.4	49.4	49.4	49.4	49.4	49.4	49.4	49.4	49.4	49.4	49.4	49.4	49.4	49.4	49.4	49.4	49.4	49.4	49.4	24.7	0.0	0.0	0.0	0.0	0.0
25	0.0	0.0	0.0	0.0	7.4	49.4	91.4	98.8	98.8	98.8	98.8	98.8	98.8	98.8	98.8	98.8	98.8	98.8	98.8	98.8	98.8	98.8	98.8	98.8	91.4	49.4	7.4	0.0	0.0	0.0	0.0
30	0.0	0.0	0.0	0.0	32.1	74.1	116.1	148.2	148.2	148.2	148.2	148.2	148.2	148.2	148.2	148.2	148.2	148.2	148.2	148.2	148.2	148.2	148.2	148.2	116.1	74.1	32.1	0.0	0.0	0.0	0.0
35	0.0	0.0	0.0	14.8	56.8	98.8	140.8	182.8	197.6	197.6	197.6	197.6	197.6	197.6	197.6	197.6	197.6	197.6	197.6	197.6	197.6	197.6	197.6	182.8	140.8	98.8	56.8	14.8	0.0	0.0	0.0
40	0.0	0.0	0.0	39.5	81.5	123.5	165.5	207.5	247.1	247.1	247.1	247.1	247.1	247.1	247.1	247.1	247.1	247.1	247.1	247.1	247.1	247.1	247.1	207.5	165.5	123.5	81.5	39.5	0.0	0.0	0.0
45	0.0	0.0	22.2	64.2	106.2	148.2	190.2	232.2	274.2	296.5	296.5	296.5	296.5	296.5	296.5	296.5	296.5	296.5	296.5	296.5	296.5	296.5	296.5	274.2	232.2	190.2	148.2	106.2	64.2	22.2	0.0
50	0.0	4.9	46.9	88.9	130.9	172.9	214.9	256.9	298.9	340.9	345.9	345.9	345.9	345.9	345.9	345.9	345.9	345.9	345.9	345.9	345.9	340.9	298.9	256.9	214.9	172.9	130.9	88.9	46.9	4.9	0.0
55	0.0	29.6	71.6	113.6	155.6	197.6	239.6	281.6	323.6	365.6	395.3	395.3	395.3	395.3	395.3	395.3	395.3	395.3	395.3	395.3	395.3	365.6	323.6	281.6	239.6	197.6	155.6	113.6	71.6	29.6	0.0
60	12.4	54.4	96.4	138.4	180.4	222.4	264.4	306.4	348.4	390.4	432.4	444.7	444.7	444.7	444.7	444.7	444.7	444.7	444.7	444.7	432.4	390.4	348.4	306.4	264.4	222.4	180.4	138.4	96.4	54.4	12.4
65	37.1	79.1	121.1	163.1	205.1	247.1	289.1	331.1	373.1	415.1	457.1	494.1	494.1	494.1	494.1	494.1	494.1	494.1	494.1	494.1	457.1	415.1	373.1	331.1	289.1	247.1	205.1	163.1	121.1	79.1	37.1
70	61.8	103.8	145.8	187.8	229.8	271.8	313.8	355.8	397.8	439.8	481.8	523.8	543.5	543.5	543.5	543.5	543.5	543.5	543.5	543.5	481.8	439.8	397.8	355.8	313.8	271.8	229.8	187.8	145.8	103.8	61.8
75	86.5	128.5	170.5	212.5	254.5	296.5	338.5	380.5	422.5	464.5	506.5	548.5	590.5	592.9	592.9	592.9	592.9	592.9	590.5	548.5	506.5	464.5	422.5	380.5	338.5	296.5	254.5	212.5	170.5	128.5	86.5
80	111.2	153.2	195.2	237.2	279.2	321.2	363.2	405.2	447.2	489.2	531.2	573.2	615.2	642.4	642.4	642.4	642.4	642.4	615.2	573.2	531.2	489.2	447.2	405.2	363.2	321.2	279.2	237.2	195.2	153.2	111.2
85	135.9	177.9	219.9	261.9	303.9	345.9	387.9	429.9	471.9	513.9	555.9	597.9	639.9	681.9	691.8	691.8	691.8	681.9	639.9	597.9	555.9	513.9	471.9	429.9	387.9	345.9	303.9	261.9	219.9	177.9	135.9
90	160.6	202.6	244.6	286.6	328.6	370.6	412.6	454.6	496.6	538.6	580.6	622.6	664.6	706.6	741.2	741.2	741.2	706.6	664.6	622.6	580.6	538.6	496.6	454.6	412.6	370.6	328.6	286.6	244.6	202.6	160.6
95	185.3	227.3	269.3	311.3	353.3	395.3	437.3	479.3	521.3	563.3	605.3	647.3	689.3	731.3	773.3	790.6	773.3	731.3	689.3	647.3	605.3	563.3	521.3	479.3	437.3	395.3	353.3	311.3	269.3	227.3	185.3
100	210.0	252.0	294.0	336.0	378.0	420.0	462.0	504.0	546.0	588.0	630.0	672.0	714.0	756.0	798.0	840.0	798.0	756.0	714.0	672.0	630.0	588.0	546.0	504.0	462.0	420.0	378.0	336.0	294.0	252.0	210.0

Table 4: Power output of all four motors at 30mph

POWER	steering angle (deg)																												
@30mph TPS (%)	-15	-14	-13	-12	-11	-10	-9	-8	-7	-6	-5	-4	-3	-2	-1	0	1	2	3	4	5	6	7	8	9	10	11	12	13	14	15
0	0.0	0.0	0.0	0.0	-1.7	-3.9	-6.1	-7.8	-7.8	-7.8	-7.8	-7.8	-7.8	-7.8	-7.8	-7.8	-7.8	-7.8	-7.8	-7.8	-7.8	-7.8	-7.8	-7.8	-6.1	-3.9	-1.7	0.0	0.0	0.0	0.0
5	0.0	0.0	0.0	0.0	-0.4	-2.6	-4.8	-5.2	-5.2	-5.2	-5.2	-5.2	-5.2	-5.2	-5.2	-5.2	-5.2	-5.2	-5.2	-5.2	-5.2	-5.2	-5.2	-5.2	-4.8	-2.6	-0.4	0.0	0.0	0.0	0.0
10	0.0	0.0	0.0	0.0	0.0	-1.3	-2.6	-2.6	-2.6	-2.6	-2.6	-2.6	-2.6	-2.6	-2.6	-2.6	-2.6	-2.6	-2.6	-2.6	-2.6	-2.6	-2.6	-2.6	-2.6	-1.3	0.0	0.0	0.0	0.0	0.0
15	0.0	0.0	0.0	0.0	0.0	0.0	0.0	0.0	0.0	0.0	0.0	0.0	0.0	0.0	0.0	0.0	0.0	0.0	0.0	0.0	0.0	0.0	0.0	0.0	0.0	0.0	0.0	0.0	0.0	0.0	0.0
20	0.0	0.0	0.0	0.0	0.0	1.3	2.6	2.6	2.6	2.6	2.6	2.6	2.6	2.6	2.6	2.6	2.6	2.6	2.6	2.6	2.6	2.6	2.6	2.6	2.6	1.3	0.0	0.0	0.0	0.0	0.0
25	0.0	0.0	0.0	0.0	0.4	2.6	4.8	5.2	5.2	5.2	5.2	5.2	5.2	5.2	5.2	5.2	5.2	5.2	5.2	5.2	5.2	5.2	5.2	5.2	4.8	2.6	0.4	0.0	0.0	0.0	0.0
30	0.0	0.0	0.0	0.0	1.7	3.9	6.1	7.8	7.8	7.8	7.8	7.8	7.8	7.8	7.8	7.8	7.8	7.8	7.8	7.8	7.8	7.8	7.8	7.8	6.1	3.9	1.7	0.0	0.0	0.0	0.0
35	0.0	0.0	0.0	0.8	3.0	5.2	7.5	9.7	10.5	10.5	10.5	10.5	10.5	10.5	10.5	10.5	10.5	10.5	10.5	10.5	10.5	10.5	10.5	9.7	7.5	5.2	3.0	0.8	0.0	0.0	0.0
40	0.0	0.0	0.0	2.1	4.3	6.5	8.8	11.0	13.1	13.1	13.1	13.1	13.1	13.1	13.1	13.1	13.1	13.1	13.1	13.1	13.1	13.1	13.1	11.0	8.8	6.5	4.3	2.1	0.0	0.0	0.0
45	0.0	0.0	1.2	3.4	5.6	7.8	10.1	12.3	14.5	15.7	15.7	15.7	15.7	15.7	15.7	15.7	15.7	15.7	15.7	15.7	15.7	15.7	14.5	12.3	10.1	7.8	5.6	3.4	1.2	0.0	0.0
50	0.0	0.3	2.5	4.7	6.9	9.2	11.4	13.6	15.8	18.1	18.3	18.3	18.3	18.3	18.3	18.3	18.3	18.3	18.3	18.3	18.3	18.1	15.8	13.6	11.4	9.2	6.9	4.7	2.5	0.3	0.0
55	0.0	1.6	3.8	6.0	8.2	10.5	12.7	14.9	17.1	19.4	20.9	20.9	20.9	20.9	20.9	20.9	20.9	20.9	20.9	20.9	20.9	19.4	17.1	14.9	12.7	10.5	8.2	6.0	3.8	1.6	0.0
60	0.7	2.9	5.1	7.3	9.5	11.8	14.0	16.2	18.4	20.7	22.9	23.5	23.5	23.5	23.5	23.5	23.5	23.5	23.5	23.5	22.9	20.7	18.4	16.2	14.0	11.8	9.5	7.3	5.1	2.9	0.7
65	2.0	4.2	6.4	8.6	10.9	13.1	15.3	17.5	19.8	22.0	24.2	26.2	26.2	26.2	26.2	26.2	26.2	26.2	26.2	26.2	24.2	22.0	19.8	17.5	15.3	13.1	10.9	8.6	6.4	4.2	2.0
70	3.3	5.5	7.7	9.9	12.2	14.4	16.6	18.8	21.1	23.3	25.5	27.7	28.8	28.8	28.8	28.8	28.8	28.8	28.8	27.7	25.5	23.3	21.1	18.8	16.6	14.4	12.2	9.9	7.7	5.5	3.3
75	4.6	6.8	9.0	11.3	13.5	15.7	17.9	20.1	22.4	24.6	26.8	29.0	31.3	31.4	31.4	31.4	31.4	31.4	31.3	29.0	26.8	24.6	22.4	20.1	17.9	15.7	13.5	11.3	9.0	6.8	4.6
80	5.9	8.1	10.3	12.6	14.8	17.0	19.2	21.5	23.7	25.9	28.1	30.3	32.6	34.0	34.0	34.0	34.0	34.0	32.6	30.3	28.1	25.9	23.7	21.5	19.2	17.0	14.8	12.6	10.3	8.1	5.9
85	7.2	9.4	11.6	13.9	16.1	18.3	20.5	22.8	25.0	27.2	29.4	31.7	33.9	36.1	36.6	36.6	36.6	36.1	33.9	31.7	29.4	27.2	25.0	22.8	20.5	18.3	16.1	13.9	11.6	9.4	7.2
90	8.5	10.7	13.0	15.2	17.4	19.6	21.8	24.1	26.3	28.5	30.7	33.0	35.2	37.4	39.2	39.2	39.2	37.4	35.2	33.0	30.7	28.5	26.3	24.1	21.8	19.6	17.4	15.2	13.0	10.7	8.5
95	9.8	12.0	14.3	16.5	18.7	20.9	23.2	25.4	27.6	29.8	32.1	34.3	36.5	38.7	40.9	41.9	40.9	38.7	36.5	34.3	32.1	29.8	27.6	25.4	23.2	20.9	18.7	16.5	14.3	12.0	9.8
100	11.1	13.3	15.6	17.8	20.0	22.2	24.5	26.7	28.9	31.1	33.4	35.6	37.8	40.0	42.3	44.5	42.3	40.0	37.8	35.6	33.4	31.1	28.9	26.7	24.5	22.2	20.0	17.8	15.6	13.3	11.1

This map can be considered a sufficient starting point for a vehicle with fully functional four-wheel torque vectoring. However, it is intended to be further developed to tailor to specific vehicle parameters and driver preferences and should still need fine tuning in practice.

The torques determined in the maps were input into the simulation to output MMDs based on throttle input. Figures 22 and 23 below show the changes to the MMD when throttle position is at 0, 15 (neutral), 45, 75, and 100 percent respectively, at 0 degrees and 3 degrees of vehicle slip, respectively. Notably, the peak Ay and Cn values do not reduce significantly when throttle position is increased. This can be attributed to the map prioritizing TV over absolute motor torque at higher steering angles, even under maximum throttle input.

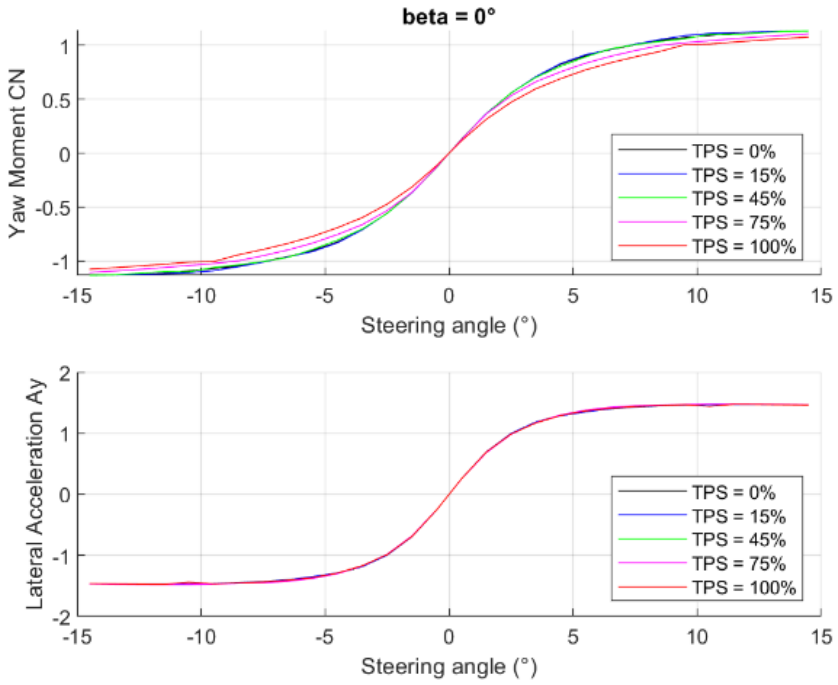

Figure 22: Cn and Ay versus steering angle plots at various throttle positions at 0° vehicle slip

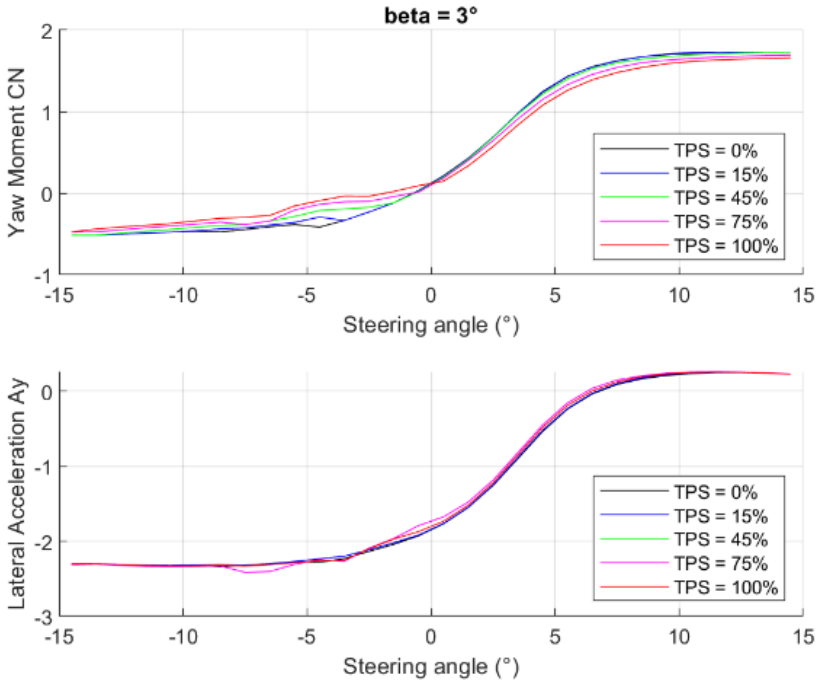

Figure 23: Cn and Ay versus steering angle plots at various throttle positions at 3° vehicle slip

CHAPTER VII

CONCLUSION

The simulation is built upon existing vehicle modeling equations but expanded to create Milliken Moment Diagram (MMD) simulations that accommodate torque vectoring. The resulting code is a vehicle model which now can quantify the effects of adding or modifying TV. Several torque vectoring configurations were analyzed with this simulation, and the results were compared. From the analysis, adding torque vectoring significantly improved yaw rate with respect to steering input. This is concisely illustrated in Figures 16 and 17 on page 32. In addition, several conditions were varied to observe how the MMD reacts to the changes.

The code that comprises this simulation is also intended to be a basis to create motor control maps prior to testing the vehicle. It is set up to accommodate changes to the vehicle and tire models. Through iteration with real-world testing, the model can be utilized to calculate optimal torque commanded to each motor for a given vehicle.

CHAPTER VIII

FUTURE WORK

While the hypothesized trends are visible in the results, there are still many opportunities to further refine the models in the simulation, including, but not limited to, the suggestions below. The suspension model in the simulation is rudimentary and could benefit from being parameterized as a proper spring-and-damper system. The case where this is most evident is when excessive vehicle roll causes the inside wheels to lift off the ground. While wheel lift-off is inevitable in certain vehicle setups, it is currently simulated as an abrupt transition, when it is more gradual in practice. In addition, the simulations may affect vehicle stability when a wheel is lifted off the ground, which may require future attention in the testing phase.

The aerodynamic model is set up to be a proof of concept for a car with downforce-producing elements and could be improved further. A variable not considered in this simulation but could have a significant effect is downforce relative to vehicle attitude, such as slip about the yaw axis. This takes extensive computational effort to simulate, but this is often already accomplished when designing a comprehensive aero package for a vehicle.

The simulation created lays the groundwork to better understand the handling and yaw behavior of a vehicle with or without torque vectoring and can

be used to improve vehicle functions, such as torque vectoring gains, prior to physical testing if utilized in a design of experiments (DOE). If being used for practical purposes, the tire models and vehicle parameters will need updated to what is intended in the design. An example of data being used to affect torque vectoring can be found in [26]. When these models are further refined, and validated through testing, the ability to fully optimize the TV controls and map of the motors becomes more achievable.

BIBLIOGRAPHY

[1] W.F. Milliken and D.L. Milliken. (1995). *Race Car Vehicle Dynamics*. Society of Automotive Engineers.

[2] H.B. Pacejka. (2012). *Tire and Vehicle Dynamics, 3rd edition*. Butterworth-Heinemann. Oxford.

[3] T.D. Gillespie. (1994). *Fundamentals of Vehicle Dynamics.* Society of Automotive Engineers.

[4] J.Y. Wong. (2008). *Theory of Ground Vehicles*. John Wiley and Sons, Inc.

[5] R. Rajamani. (2012). *Vehicle Dynamics and Control.* Springer.

[6] R. Gross. *FSAE Racing Vehicle Dynamics.* The University of Akron. Unpublished Manuscript.

[7] L. Segal. (1956). Theoretical Prediction and *Experimental Substantiation of the Response of the Automobile to Steering Control*. The Institute of Mechanical Engineers, pp. 310-330.

[8] W.F. Milliken, F. Dell'Amico, and R.S. Rice. (1976). *The Static Directional Stability and Control of the Automobile.* Society of Automotive Engineers. SAE Paper No. 760712.

[9] R.S. Rice and W.F. Milliken. (1980). *Static Stability and Control of the Automobile Utilizing the Moment Method*. Society of Automotive Engineers. SAE Paper No. 800847.

[10] C. Patton. (2013). *Development of Vehicle Dynamics Tools for Motorsports.* Oregon State University. PhD Dissertation.

[11] H.S. Radt and W.F. Milliken. (1960). *Motions of Skidding Automobiles*. Society of Automotive Engineering. SAE Paper No. 600133.

[12] H.S. Radt and D.A. Glemming. (1993). *Normalization of Tire Force and Moment Data*. Tire Science and Technology. vol. 21, pp. 91-119.

[13] H.S. Radt. (1995). *Processing of Tire Force & Moment Data.* Society of Automotive Engineers. SAE Paper No. 951048.

[14] H.S. Radt. (1994). *An Efficient Method for Treating Race Tire Force-Moment Data*. Society of Automotive Engineers. SAE Paper No. 942536.

[15] TNO. (2001). *MF-Tyre User Manual Version 5.2.* The Netherlands. Delft-Tyre.

[16] J.E. Gorcya. (2010). *Force & Moment Plots from Pacejka 2002 Magic Formula Tire Model Coefficients*. TARDEC.

[17] E. Bakker, L. Nyborg, and H.B. Pacejka. (1987). *Tyre Modelling for Use in Vehicle Dynamics Studies*. Society of Automotive Engineers, SAE Paper No. 870421.

[18] M. Blundell and D. Harty. (2004). *The Multibody Systems Approach to Vehicle Dynamics*. Elsevier Butterworth-Heinemann. Oxford.

[19] B. Siegler, A. Deakin, and D. Crolla. (2000). *Lap Time Simulation: Comparison of Steady State, Quasi-Static and Transient Racing Car Cornering Strategies*. The University of Leeds. Society of Automotive Engineers. SAE Paper No. 2000-01-3563.

[20] *Vehicle Dynamics Terminology*. (1976). Society of Automotive Engineers. Warendal, PA, SAE Standard J760e.

[21] *Coordinate Systems in Vehicle Dynamics Blockset.* (2008). Mathworks.

[22] Y. Ye, L. He, and Q. Zhang. (2016). *Steering Control Strategies for a Four-Wheel-Independent-Steering Bin Managing Robot*. IFAC 49-16 (2016) 039-044

[23] M. Makatchev, J.J. McPhee, S.K. Tso and S.Y.T. Lang. (2002). *System Design, Modelling, and Control of a Four-Wheel-Steering Mobile Robot. University of Hong Kong.*

[24] AMK. (2018). *DD5-14-10-POW Formula Student Motor Data Sheet*.

[25] E.M. Kasprzak and D. Gentz. (2006). *The Formula SAE Tire Test Consortium-Tire Testing and Data Handling*. Society of Automotive Engineers, SAE Paper No. 2006-01-3606.

[26] J. Ryu and J.C. Gerdes. (2004). *Integrating Inertial Sensors with GPS for Vehicle Dynamics Control.* Stanford University. Journal of Dynamic Systems, Measurement, and Control.

APPENDICES

APPENDIX A

TIRE MODEL CODE

```
function [Fx,Fy,Mx,My,Mz] = Goodyear_20x7_13_7in_12psi_V43(Fz,Vx,gamma,alpha,kappa,side)

    %% Input values to test w/o function
    %clear,clc;
    %Fz = 500;              % vertical force on tire
    %Vx = 25;               % Wheel velocity (mph)
    %gamma = 0;             % Positive inclination angle
    %alpha_deg = linspace(-10,10);
    %alpha = alpha_deg*pi/180;             % Positive slip angle
    %kappa = 0;             % Longitudinal slip (ratio)

    %% TIR file of D2704
    FILE_TYPE               ='tir';
    FILE_VERSION            = 3.0;
    FILE_FORMAT             ='ASCII';
    % : TIRE_VERSION :      PAC2002
    % : COMMENT :           Stackpole Engineering Services, Inc.
    % : COMMENT :           Created By : Melissa Patterson
    % : COMMENT :           August 31, 2012
    % : COMMENT :           Customer     : FSAE
    % : COMMENT :           Construction : 20.0x7-13 7in
    % : COMMENT :           DOT : XXXXXX
    % : COMMENT :           Position     : All
    % : COMMENT :           Manufacturer : Goodyear
    % : COMMENT :           Nom. section width(in)  7.00
    % : COMMENT :           Nom. aspect ratio        0.5
    % : COMMENT :           Infl. pressure   (Psi)  12.0
    % : COMMENT :           Rim Diameter      (in)  13.0
    % : COMMENT :           Rim Width         (in)   7.0
    % : COMMENT :           Test speed       (mph)  25.0
    % : FILE FORMAT :       ASCII
    %
    % USE_MODE specifies the type of calculation performed:
    %       0: Fz only, no Magic Formula evaluation
    %       1: Fx,My only
    %       2: Fy,Mx,Mz only
    %       3: Fx,Fy,Mx,My,Mz uncombined force/moment calculation
    %       4: Fx,Fy,Mx,My,Mz combined force/moment calculation
    %     +10: including relaxation behavior
    %     *-1: mirroring of tyre characteristics
    %
    %       example: USE_MODE = -12 implies:
    %       -calculation of Fy,Mx,Mz only
    %       -including relaxation effects
    %       -mirrored tyre characteristics
    %
    %-----------------------------------------------------ses_tire_plotter
    %[SES_TIRE_PLOTTER]
    YEAR                    = 2012;
    MANUFACTURER            = 'Goodyear';
    CONSTRUCTION            = '20.0x7-13 7in';
    RIM_DIAMETER_INCH       = 13.0; %in
    RIM_WIDTH_INCH          = 7.0; %in
    INFLATION_PSI           = 12.0;
    %-----------------------------------------------------------------units
    %[UNITS]
    LENGTH              = 'meter';
    FORCE               = 'Newton';
    ANGLE               = 'radians';
    MASS                = 'kg';
    TIME                = 'second';
```

```
%-----------------------------------------------------------------model
%[MODEL]
PROPERTY_FILE_FORMAT     ='PAC2002';
USE_MODE                 = 4       ;            %Tyre use switch (IUSED)
VXLOW                    = 1;
LONGVL                   = 11.1760;             %Measurement speed
TYRESIDE                 = 'RIGHT';             %Mounted side of tyre at vehicle/test bench
%-------------------------------------------------------------dimensions
%[DIMENSION]
UNLOADED_RADIUS          = 0.2540;              %Free tyre radius
WIDTH                    = 0.1778;              %Nominal section width of the tyre
ASPECT_RATIO             = 0.5000;              %Nominal aspect ratio
RIM_RADIUS               = 0.1651;              %Nominal rim radius
RIM_WIDTH                = 0.1778;              %Rim width
%-----------------------------------------------------------------shape
%[SHAPE]
%{radial width}
% 1.0    0.0
% 1.0    0.4
% 1.0    0.9
% 0.9    1.0
%-------------------------------------------------------------parameter
%[VERTICAL]
VERTICAL_STIFFNESS       = 114177.00;           %Tyre vertical stiffness
VERTICAL_DAMPING         = 57088.5;             %Tyre vertical damping
BREFF                    = 0.2540;              %Low load stiffness e.r.r.
DREFF                    = 0.2440;              %Peak value of e.r.r.
FREFF                    = 0.3000;              %High load stiffness e.r.r.
FNOMIN                   = 557.1984;            %Nominal wheel load
%-----------------------------------------------------long_slip_range
%[LONG_SLIP_RANGE]
KPUMIN                   = -0.5000;             %Minimum valid wheel slip
KPUMAX                   =  0.5000;             %Maximum valid wheel slip
%-----------------------------------------------slip_angle_range
%[SLIP_ANGLE_RANGE]
ALPMIN                   = -0.2094;             %Minimum valid slip angle
ALPMAX                   =  0.2094;             %Maximum valid slip angle
%-------------------------------------------inclination_slip_range
%[INCLINATION_ANGLE_RANGE]
CAMMIN                   = 0.0000;             %Minimum valid camber angle
CAMMAX                   =  0.0698;            %Maximum valid camber angle
%-----------------------------------------------vertical_force_range
%[VERTICAL_FORCE_RANGE]
FZMIN                    =    222.4;            %Minimum allowed wheel load
FZMAX                    =   1556.8;            %Maximum allowed wheel load
%-----------------------------------------------------------------scaling
%[SCALING_COEFFICIENTS]
LFZO                    = 1.0;                  %Scale factor of nominal (rated) load
LCX                     = 1.0;                  %Scale factor of Fx shape factor
LMUX                    = 1.0;                  %Scale factor of Fx peak friction coefficient
LEX                     = 1.0;                  %Scale factor of Fx curvature factor
LKX                     = 1.0;                  %Scale factor of Fx slip stiffness
LHX                     = 1.0;                  %Scale factor of Fx horizontal shift
LVX                     = 1.0;                  %Scale factor of Fx vertical shift
LGAX                    = 1.0;                  %Scale factor of camber for Fx
LCY                     = 1.0;                  %Scale factor of Fy shape factor
LMUY                    = 1.0;                  %Scale factor of Fy peak friction coefficient
LEY                     = 1.0;                  %Scale factor of Fy curvature factor
LKY                     = 1.0;                  %Scale factor of Fy cornering stiffness
LHY                     = 1.0;                  %Scale factor of Fy horizontal shift
LVY                     = 1.0;                  %Scale factor of Fy vertical shift
LGAY                    = 1.0;                  %Scale factor of camber for Fy
LTR                     = 1.0;                  %Scale factor of peak of pneumatic trail
LRES                    = 1.0;                  %Scale factor for offset of residual torque
LGAZ                    = 1.0;                  %Scale factor of camber for Mz
LXAL                    = 1.0;                  %Scale factor of alpha influence on Fx
LYKA                    = 1.0;                  %Scale factor of alpha influence on Fx
LVYKA                   = 1.0;                  %Scale factor of kappa induced Fy
LS                      = 1.0;                  %Scale factor of moment arm of Fx
LSGKP                   = 1.0;                  %Scale factor of relaxation length of Fx
LSGAL                   = 1.0;                  %Scale factor of relaxation length of Fy
LGYR                    = 1.0;                  %Scale factor of gyroscopic torque
LMX                     = 1.0;                  %Scale factor of overturning couple
LVMX                    = 1.0;                  %Scale factor of Mx vertical shift
LMY                     = 1.0;                  %Scale factor of rolling resistance torque
%-----------------------------------------------------------LONGITUDINAL_FORCE
%[LONGITUDINAL_COEFFICIENTS]
PCX1                    =  1.94332170E+00;      %Shape factor Cfx for longitudinal force
PDX1                    = -2.75883780E+00;      %Longitudinal friction Mux at Fznom
```

```
PDX2                    =  1.13304780E-01;      %Variation of friction Mux with load
PDX3                    =  4.53981670E+00;      %Variation of friction Mux with camber
PEX1                    =  7.31181520E-01;      %Longitudinal curvature Efx at Fznom
PEX2                    = -6.12034860E-18;      %Variation of curvature Efx with load
PEX3                    = -5.30219090E-16;      %Variation of curvature Efx with load squared
PEX4                    =  2.59460030E-02;      %Factor in curvature Efx while driving
PKX1                    =  5.02759950E+01;      %Longitudinal slip stiffness Kfx/Fz at Fznom
PKX2                    =  3.24391120E-06;      %Variation of slip stiffness Kfx/Fz with load
PKX3                    = -2.12216770E-02;      %Exponent in slip stiffness Kfx/Fz with load
PHX1                    =  3.78973130E-03;      %Horizontal shift Shx at Fznom
PHX2                    =  1.47266430E-02;      %Variation of shift Shx with load
PVX1                    =  4.37805190E-02;      %Vertical shift Svx/Fz at Fznom
PVX2                    = -2.21771300E-02;      %Variation of shift Svx/Fz with load
RBX1                    =  5.44487250E+02;      %Slope factor for combined slip Fx reduction
RBX2                    = -9.03845100E+01;      %Variation of slope Fx reduction with kappa
RBX3                    =  0;                   %not in tire data gvar('RBY4',S);
RCX1                    =  7.35031830E-01;      %Shape factor for combined slip Fx reduction
REX1                    = -5.20357270E+00;      %Curvature factor of combined Fx
REX2                    =  1.20266330E+01;      %Curvature factor of combined Fx with load
RHX1                    = -1.64576360E-02;      %Shift factor for combined slip Fx reduction
PTX1                    =  0.00000000E+00;      %Relaxation length SigKap0/Fz at Fznom
PTX2                    =  0.00000000E+00;      %Variation of SigKap0/Fz with load
PTX3                    =  0.00000000E+00;      %Variation of SigKap0/Fz with exponent of load
%----------------------------------------------------------OVERTURNING_MOMENT
%[OVERTURNING_COEFFICIENTS]
QSX1                    =  1.96429900E-02;      %Lateral force induced overturning moment
QSX2                    =  8.93865340E-01;      %Camber induced overturning couple
QSX3                    =  2.55806260E-02;      %Fy induced overturning couple
%-------------------------------------------------------------------LATERAL_FORCE
%[LATERAL_COEFFICIENTS]
PCY1                    =  1.64612450E+00;     %Shape factor Cfy for lateral forces
PDY1                    = -2.83921320E+00;     %Lateral friction Muy
PDY2                    =  1.81573930E-01;     %Variation of friction Muy with load
PDY3                    =  3.37512120E+00;     %Variation of friction Muy with squared camber
PEY1                    =  8.52594570E-01;     %Lateral curvature Efy at Fznom
PEY2                    =  8.01297920E-03;     %Variation of curvature Efy with load
PEY3                    = -4.24941250E-01;     %Zero order camber dependency of curvature Efy
PEY4                    =  5.98168410E-01;     %Variation of curvature Efy with camber
PEY5                    =  0;
PKY1                    = -8.23100440E+01;     %Maximum value of stiffness Kfy/Fznom
PKY2                    =  2.31834620E+00;     %Load at which Kfy reaches maximum value
PKY3                    = -3.68275220E-01;     %Variation of Kfy/Fznom with camber
PKY4                    =  2;
PKY5                    =  0;
PHY1                    =  9.64884930E-05;     %Horizontal shift Shy at Fznom
PHY2                    =  7.70517930E-04;     %Variation of shift Shy with load
PHY3                    =  5.07400640E-02;     %Variation of shift Shy with camber
PVY1                    = -2.57500330E-02;     %Vertical shift in Svy/Fz at Fznom
PVY2                    = -9.44018580E-04;     %Variation of shift Svy/Fz with load
PVY3                    = -1.92383650E-02;     %Variation of shift Svy/Fz with camber
PVY4                    = -1.24883410E-01;     %Variation of shift Svy/Fz with camber and load
RBY1                    =  6.51303130E+00;     %Slope factor for combined Fy reduction
RBY2                    = -1.15949550E-03;     %Variation of slope Fy reduction with alpha
RBY3                    =  1.62736530E+01;     %Shift term for alpha in slope Fy reduction
RBY4                    =  0;                  %not in tire data gvar('RBY4',S);
RCY1                    =  1.99443930E+00;     %Shape factor for combined Fy reduction
REY1                    =  1.59266480E+00;     %Curvature factor of combined Fy
REY2                    =  9.80528380E-03;     %Curvature factor of combined Fy with load
RHY1                    =  1.45762450E-02;     %Shift factor for combined Fy reduction
RHY2                    =  1.12761620E-02;     %Shift factor for combined Fy reduction with load
RVY1                    = -4.14295630E-02;     %Kappa induced side force Svyk/Muy*Fz at Fznom
RVY2                    =  2.17512340E-02;     %Variation of Svyk/Muy*Fz with load
RVY3                    = -4.96807380E+00;     %Variation of Svyk/Muy*Fz with camber
RVY4                    = -2.19784750E+01;     %Variation of Svyk/Muy*Fz with alpha
RVY5                    =  1.49837370E+00;     %Variation of Svyk/Muy*Fz with kappa
RVY6                    =  1.42984740E+00;     %Variation of Svyk/Muy*Fz with atan (kappa)
PTY1                    =  0.00000000E+00;     %Peak value of relaxation length SigAlp0/R0
PTY2                    =  0.00000000E+00;     %Value of Fz/Fznom where SigAlp0 is extreme
%-----------------------------------------------------ROLLING_COEFFICIENTS
%[ROLLING_COEFFICIENTS]
QSY1                    = 0.00000000E+00 ;     %Rolling resistance torque coefficien)
QSY2                    = 0.00000000E+00 ;     %Rolling resistance torque depending on Fx
QSY3                    = 0.00000000E+00 ;     %Rolling resistance torque depending on speed
QSY4                    = 0.00000000E+00 ;     %Rolling resistance torque depending on speed ^4
%-----------------------------------------------------------ALIGNING_TORQUE
%[ALIGNING_COEFFICIENTS]
QBZ1                    =  1.20188460E+00;     %Trail slope factor for trail Bpt at Fznom
QBZ2                    =  1.29852600E-01;     %Variation of slope Bpt with load
QBZ3                    =  5.51415720E-02;     %Variation of slope Bpt with load squared
```

```
QBZ4                    = -9.29896380E+00;     %Variation of slope Bpt with camber
QBZ5                    =  8.67090690E+00;     %Variation of slope Bpt with absolute camber
QBZ9                    =  1.48134320E-02;     %Slope factor Br of residual torque Mzr
QBZ10                   =  1.01155280E-03;     %Slope factor Br of residual torque Mzr
QCZ1                    =  5.75536270E+00;     %Shape factor Cpt for pneumatic trail
QDZ1                    =  4.52175120E-02;     %Peak trail Dpt" = Dpt*(Fz/Fznom*R0)
QDZ2                    =  1.24910010E-02;     %Variation of peak Dpt" with load
QDZ3                    =  3.06196910E-02;     %Variation of peak Dpt" with camber
QDZ4                    =  5.25084820E-02;     %Variation of peak Dpt" with camber squared
QDZ6                    = -2.73726840E-02;     %Peak residual torque Dmr" = Dmr/(Fz*R0)
QDZ7                    = -2.57458700E-02;     %Variation of peak factor Dmr" with load
QDZ8                    = -2.82180820E-02;     %Variation of peak factor Dmr" with camber
QDZ9                    = -2.15225170E-02;     %Variation of peak factor Dmr" with camber and load
QEZ1                    = -1.70417910E+01;     %Trail curvature Ept at Fznom
QEZ2                    =  1.35057580E+01;     %Variation of curvature Ept with load
QEZ3                    = -4.87940590E-01;     %Variation of curvature Ept with load squared
QEZ4                    = -3.59374280E-01;     %Variation of curvature Ept with sign of Alpha-t
QEZ5                    =  8.93593140E+00;     %Variation of Ept with camber and sign Alpha-t
QHZ1                    =  3.95025070E-03;     %Trail horizontal shift Sht at Fznom
QHZ2                    = -8.74135150E-03;     %Variation of shift Sht with load
QHZ3                    =  4.23196360E-03;     %Variation of shift Sht with camber
QHZ4                    = -1.06176910E-02;     %Variation of shift Sht with camber and load
SSZ1                    =  0.00000;            %Nominal value of s/R0: effect of Fx on Mz
SSZ2                    =  0.00000;            %Variation of distance s/R0 with Fy/Fznom
SSZ3                    =  0.00000;            %Variation of distance s/R0 with camber
SSZ4                    =  0.00000;            %Variation of distance s/R0 with load and camber
QTZ1                    =  0;                  %Gyration torque constant
MBELT                   =  0;                  %Belt mass of the wheel

%% Flip coefficients if side is left instead of right
if side == 'l'
    RHX1 = -RHX1;
    QSX1 = -QSX1;
    PEY3 = -PEY3;
    PHY1 = -PHY1;
    PHY2 = -PHY2;
    PVY1 = -PVY1;
    PVY2 = -PVY2;
    RBY3 = -RBY3;
    RVY1 = -RVY1;
    RVY2 = -RVY2;
    QBZ4 = -QBZ4;
    QDZ3 = -QDZ3;
    QDZ6 = -QDZ6;
    QDZ7 = -QDZ7;
    QEZ4 = -QEZ4;
    QHZ1 = -QHZ1;
    QHZ2 = -QHZ2;
    SSZ1 = -SSZ1;
end


    %% Calculations
Fz0 = FNOMIN;
R0 = UNLOADED_RADIUS;
    dfz = (Fz - Fz0)./Fz;

    %% Long Combined Slip (pure slip Gxa=1)
    % logic added to mirror SHXa near RHX1 to work around Gxa asymptote issue
%SHxa = RHX1 * sign(abs(alpha + RHX1) -.05);
SHxa = 1.5; %dummy constant

%SHxa = RHX1;
    alpha_s = alpha + SHxa;
    Bxa = (RBX1+RBX3.*gamma.^2).*cos(atan(RBX2.*kappa)).*LXAL;
    Cxa = RCX1;
    Exa = REX1+REX2.*dfz;
    Gxa = (cos(Cxa.*atan(Bxa.*alpha_s-Exa.*(Bxa.*alpha_s-atan(Bxa.*alpha_s))))))...
                    ./(cos(Cxa.*atan(Bxa.*SHxa-Exa.*(Bxa.*SHxa-atan(Bxa.*SHxa))))));

%   if kappa == 0
%       Gxa = 0;
%   end

    %% Longitudinal force Fx
    SHx = (PHX1+PHX2.*dfz).*LHX;
    SVX = Fz.*(PVX1+PVX2.*dfz).*LVX.*LMUX;

    kappa_x = kappa + SHx;
```

```
    mu_x = (PDX1+PDX2.*dfz).*(1-PDX3.*(gamma).^2).*LMUX;
    Kxk = (PKX1 + PKX2.*dfz()).*exp(PKX3.*dfz()).*Fz.*LKX;

    Cx = PCX1.*LCX;
    Dx = mu_x.*Fz;
    Ex = (PEX1+PEX2.*dfz+PEX3.*dfz.^2).*(1-PEX4.*sign(kappa_x)).*LEX;
    Bx = Kxk./(Cx.*Dx);

    Fx = (Dx.*sin(Cx.*atan(Bx.*kappa_x-Ex.*(Bx.*kappa_x-atan(Bx.*kappa_x))))+SVX).*Gxa;


    %% Lateral force Fy
    mu_y = (PDY1+PDY2.*dfz).*(1-PDY3.*gamma.^2).*LMUY;

Kya = PKY1.*Fz0.*sin(PKY4.*atan(Fz./(PKY2+PKY5.*gamma.^2)./Fz0./LFZO))...
                    .*(1-PKY3.*abs(gamma)).*LKY;
    Kyg = (PVY3+PVY4.*dfz).*Fz;

SVy0 = Fz.*(PVY1+PVY2.*dfz).*LVY.*LMUY;
    SVyg = Fz.*(PVY3+PVY4.*dfz).*gamma.*LKY.*LMUY;
    SHy0 = (PHY1+PHY2.*dfz).*LHY;
    SHyg = (Kyg.*gamma - SVyg)./Kya;
    SHy = SHy0 + SHyg;
SVy = SVy0 + SVyg;

    alpha_y = alpha + SHy;

    Cy = PCY1.*LCY;
    Dy = mu_y.*Fz;
    Ey = (PEY1+PEY2.*dfz).*(1+PEY5.*gamma.^2-(PEY3+PEY4.*gamma).*sign(alpha_y)).*LEY;
    By = Kya./(Cy.*Dy);

    Fyp = (Dy.*sin(Cy.*atan(By.*alpha_y-Ey.*(By.*alpha_y-atan(By.*alpha_y))))+SVy);


    %% Lat Combined Slip (pure slip SVyk=0, Gyk=1)
    SHyk = RHY1 + RHY2.*dfz;
    kappa_s = kappa + SHyk;

    Byk = (RBY1+RBY4.*gamma.^2).*cos(atan(RBY2.*(alpha-RBY3))).*LYKA;
    Cyk = RCY1;
    Eyk = REY1 + REY2.*dfz;

    DVyk = mu_y.*Fz.*(RVY1+RVY2.*dfz+RVY3.*gamma).*cos(atan(RVY4.*alpha));
    SVyk = DVyk.*sin(RVY5.*atan(RVY6.*kappa)).*LVYKA;

    Gyk = cos(Cyk.*atan(Byk.*kappa_s-Eyk.*(Byk.*kappa_s-atan(Byk.*kappa_s))))...
                    ./cos(Cyk.*atan(Byk.*SHyk-Eyk.*(Byk.*SHyk-atan(Byk.*SHyk))));

    %% Lateral force Fy
    Fy = Gyk.*Fyp + SVyk;


    %% Overturning Moment Mx
    Mx = R0.*Fz.*LMX.*(QSX1.*LMX - QSX2.*gamma + QSX3.*Fy./Fz0);


    %% Rolling Resistance Moment My
    %My = -R0.*Fz0.*LMY.*(QSY1 + QSY2.*Fx./Fz0 + QSY3.*abs(Vx./LONGVL)...
                    %+ QSY4.*(Vx./LONGVL).^4);
    My = R0.*(SVX + kappa_x.*SHx);


    %% Self aligning moment Mz
    gamma_z = gamma.*LGAZ;
    SHt = QHZ1 + QHZ2.*dfz + (QHZ3+QHZ4.*dfz).*(gamma_z);
Ky = PKY1.*Fz0.*sin(PKY4.*atan(Fz./(PKY2+PKY5.*gamma.^2)./Fz0./LFZO))...
       .*(1 - PKY3.*abs(gamma)).*LKY;
    SHf = SHy + SVy./Ky;
    alpha_t = alpha + SHt;
    alpha_r = alpha + SHf;

    Bt = (QBZ1+QBZ2.*dfz+QBZ3.*dfz.^2).*(1+QBZ4.*gamma_z+QBZ5.*abs(gamma_z)).*LKY./LMUY;
    Ct = QCZ1;
    Dt = Fz.*(QDZ1+QDZ2.*dfz).*(1+QDZ3.*gamma_z+QDZ4.*gamma_z.^2).*(R0./Fz0).*LTR;
    Et = (QEZ1+QEZ2.*dfz+QEZ3.*dfz.^2).*(1+(QEZ4+...
                    QEZ5.*gamma_z).*(2./pi).*atan(Bt.*Ct.*alpha_t));

%if Et > ones(size(Et))
```

```
        %       warning(['Et = ' Et ' which is greater than one.']);
        %end

        Br = QBZ9.*LKY./LMUY + QBZ10.*By.*Cy;
        Cr = 1;
        Dr = Fz.*((QDZ6+QDZ7.*dfz).*LRES + (QDZ8+QDZ9.*dfz).*gamma_z).*R0.*LMUY;
        Mzr = Dr.*cos(Cr.*atan(Br.*alpha_r)).*cos(alpha);

        t = Dt.*cos(Ct.*atan(Bt.*alpha_t-Et.*(Bt.*alpha_t-atan(Bt.*alpha_t)))).*cos(alpha);

        Mz = -t.*Fy + Mzr;

    %% logic added for zero crossing
    if Fz <= 0.1
        Fx = 0;
        Fy = 0;
        Mx = 0;
        My = 0;
        Mz = 0;
    end

        %% test plot
    %figure(1)
    %plot(alpha_deg,Mz)


end
```

APPENDIX B

VEHICLE SIMULATION CODE

```
% TV Yaw Rate calculator
% by Chris Chatfield - 2022-03-06
% Updated 2023-02-12
clear, clc;

%% Initial vehicle constants
g = 9.81;               % gravitational constant (m/s^2)
Ut = 1.7;               % tire coeff of friction
m = 300;                % Total mass of car + driver (kg)
W = m * g;              % weight of car + driver (N)
L = 1.53;               % wheelbase (m)
t = 1.22;               % vehicle track width (m)
t_f = t;
t_r = t;
total_width = 1.45;     % vehicle total width (m)
Hcg = 0.295;            % CG height (m)
Rwr = 0.51;             % Rear weight ratio
Fwr = 1 - Rwr;          % Front weight ratio
Rt = .256;              % tire height (m)
Ct = 2*pi*Rt;           % tire circumference (m)
gear = 10;              % gearbox gear reduction ratio
B_rs = 0.52;            % rear roll stiffness fraction

pr = 0.3;              % relaxation coefficient for yaw iteration

dFzf_dAxb = Hcg * m / (2*L);
dFzf_dAyb = Hcg * W * (1 - B_rs) / t_f;
dFzr_dAyb = Hcg * W * B_rs / t_r;

% motor properties
peak_torque = 21;         % peak torque (N-m)
peak_power = 35E3;                % peak power (W)
peak_TW = peak_torque * gear; % peak torque at wheels after gearing

%% weight transfer calc
Wf = Fwr * W;           % Weight of front (N)
Wr = Rwr * W;           % Weight of rear (N)
a = Wr * L / W;         % CG dist from front axle (m)
b = Wf * L / W;         % CG dist from rear axle (m)

% tire contact patch coordinates (Ypos to left)
Y_fl_b = t_f/2;
Y_fr_b = -Y_fl_b;
Y_rl_b = t_r/2;
Y_rr_b = -Y_rl_b;

X_fl_b = a;
X_fr_b = X_fl_b;
X_rl_b = -b;
X_rr_b = X_rl_b;

r = 8.35;               % radius of turn (m)
Cf = 750;               % front cornering force (N/deg)
Cr = 250;               % rear cornering force (N/deg)
Vx_mph = 30;            % body velocity (mph)
Vx = Vx_mph * 0.44704;  % body velocity (m/s)

% aero loads
Fadf = 0.202*(Vx_mph^2);             % Front axle downforce (N)
Radf = 0.317*(Vx_mph^2);            % Rear axle downforce (N)
DF = Fadf + Radf;
```

```
% wheel velocities, infinite radius corner
Vx_fl = Vx; % * 7.74 / 8.35;
Vx_fr = Vx; % * 8.96 / 8.35;
Vx_rl = Vx_fl;
Vx_rr = Vx_fr;


%% vehicle slip and steer angle generation, with TV proportional to steering angle delta
tv_to_delta_deg_ratio = 21; %21
tvd = tv_to_delta_deg_ratio * 180/pi();

betas_deg = -11:1:11;     % vehicle slip grid
deltas_deg = -15:1:15;    % front steer angle grid, assuming rear delta = 0

betas = betas_deg * pi/180;
deltas = deltas_deg * pi/180;

Cn_mat = zeros(size(betas,2),size(deltas,2));
Ax_mat = zeros(size(betas,2),size(deltas,2));
Ay_mat = zeros(size(betas,2),size(deltas,2));
i_mat = zeros(size(betas,2),size(deltas,2));

b = 1;
for beta = betas
    d = 1;

    % convert corner coordinates to velocity frame
    X_fl_v = X_fl_b*cos(beta) + Y_fl_b*sin(beta);
    X_fr_v = X_fr_b*cos(beta) + Y_fr_b*sin(beta);
    X_rl_v = X_rl_b*cos(beta) + Y_rl_b*sin(beta);
    X_rr_v = X_rr_b*cos(beta) + Y_rr_b*sin(beta);

    Y_fl_v = Y_fl_b*cos(beta) - X_fl_b*sin(beta);
    Y_fr_v = Y_fr_b*cos(beta) - X_fr_b*sin(beta);
    Y_rl_v = Y_rl_b*cos(beta) - X_rl_b*sin(beta);
    Y_rr_v = Y_rr_b*cos(beta) - X_rr_b*sin(beta);

    for delta = deltas

        % initial Fz estimate - no weight transfer
        Fz_fl = (Wf + Fadf) / 2;
        Fz_fr = (Wf + Fadf) / 2;
        Fz_rl = (Wr + Radf) / 2;
        Fz_rr = (Wr + Radf) / 2;

        Ay = 0;
        omega = 0;
        % calculate torque command for steering angle
        TW = min(abs(tvd*delta),peak_TW)*sign(delta);
        %TWs(d) = TW;

        i = 1; % iteration count
        converge = 0;
        while converge == 0 && i<100

            beta_fl = atan((Vx*sin(beta) + omega*X_fl_v) / (Vx*cos(beta) - omega*Y_fl_v));
            beta_fr = atan((Vx*sin(beta) + omega*X_fr_v) / (Vx*cos(beta) - omega*Y_fr_v));
            beta_rl = atan((Vx*sin(beta) + omega*X_rl_v) / (Vx*cos(beta) - omega*Y_rl_v));
            beta_rr = atan((Vx*sin(beta) + omega*X_rr_v) / (Vx*cos(beta) - omega*Y_rr_v));

            % slip angle on each tire
            alpha_fl = beta_fl - delta;
            alpha_fr = beta_fr - delta;
            alpha_rl = beta_rl;
            alpha_rr = beta_rr;

            % slip ratio on each tire based on TW and normal load
            SR_fl = TW_to_SR(-TW,Fz_fl,Vx_fl,alpha_fl,'l');
            SR_fr = TW_to_SR( TW,Fz_fr,Vx_fr,alpha_fr,'r');
            SR_rl = TW_to_SR(-TW,Fz_rl,Vx_rl,alpha_rl,'l');
            SR_rr = TW_to_SR( TW,Fz_rr,Vx_rr,alpha_rr,'r');

%             if Fz_fl < 1 || Fz_fr < 1 || Fz_rl < 1 || Fz_rr < 1
%                 SR_fl = 0.1*sign(SR_fl);
%                 SR_fr = 0.1*sign(SR_fr);
%                 SR_rl = 0.1*sign(SR_rl);
%                 SR_rr = 0.1*sign(SR_rr);
%             end
```

```
            % apply tire model to get F&M's for each tire
            [Fx_fl,Fy_fl,Mx_fl,My_fl,Mz_fl] =
GY_20x7_13_7in_12psi_V43(Fz_fl,Vx_fl,0,alpha_fl,SR_fl,'l');
            [Fx_fr,Fy_fr,Mx_fr,My_fr,Mz_fr] =
GY_20x7_13_7in_12psi_V43(Fz_fr,Vx_fr,0,alpha_fr,SR_fr,'r');
            [Fx_rl,Fy_rl,Mx_rl,My_rl,Mz_rl] =
GY_20x7_13_7in_12psi_V43(Fz_rl,Vx_rl,0,alpha_rl,SR_rl,'l');
            [Fx_rr,Fy_rr,Mx_rr,My_rr,Mz_rr] =
GY_20x7_13_7in_12psi_V43(Fz_rr,Vx_rr,0,alpha_rr,SR_rr,'r');

            % total vehicle forces
            Fx =    Fx_fl*cos(delta) - Fy_fl*sin(delta) + ...
                    Fx_fr*cos(delta) - Fy_fr*sin(delta) + ...
                    Fx_rl + ...
                    Fx_rr;

            Fy =    Fx_fl*sin(delta) + Fy_fl*cos(delta) + ...
                    Fx_fr*sin(delta) + Fy_fr*cos(delta) + ...
                    Fy_rl + ...
                    Fy_rr;

            Mz =    X_fl_v*Fx_fl*sin(delta) - Y_fl_v*Fx_fl*cos(delta) + Y_fl_v*Fy_fl*sin(delta) +
X_fl_v*Fy_fl*cos(delta) + ...
                    X_fr_v*Fx_fr*sin(delta) - Y_fr_v*Fx_fr*cos(delta) + Y_fr_v*Fy_fr*sin(delta) +
X_fr_v*Fy_fr*cos(delta) + ...
                    -Y_rl_v*Fx_rl + X_rl_v*Fy_rl + ...
                    -Y_rr_v*Fx_rr + X_rr_v*Fy_rr;

            Ax = Fx / W;
            Ay_new = Fy / W;
            Cn = Mz / (m*g*L);

            % yaw rate iteration estimation with relaxation (ref Chris Patton eq #70)
            omega_est = Ay_new / Vx;
            omega = omega_est*(1-pr) + omega*pr;

            % calculate weight transfer based on rates
            % max statement added to avoid negative corner loads
            Fz_fl = max(Wf/2 + dFzf_dAxb * Ax + dFzf_dAyb * Ay_new + Fadf/2, 0.1);
            Fz_fr = max(Wf/2 + dFzf_dAxb * Ax - dFzf_dAyb * Ay_new + Fadf/2, 0.1);
            Fz_rl = max(Wr/2 - dFzf_dAxb * Ax + dFzr_dAyb * Ay_new + Radf/2, 0.1);
            Fz_rr = max(Wr/2 - dFzf_dAxb * Ax - dFzr_dAyb * Ay_new + Radf/2, 0.1);

            % logic to add loads back to loaded corners proportionally in case of wheel lifting
            Fz_total = Fz_fl + Fz_fr + Fz_rl + Fz_rr;
            if Fz_total > W + DF
                Fz_fl = Fz_fl * (W+DF) / Fz_total;
                Fz_fr = Fz_fr * (W+DF) / Fz_total;
                Fz_rl = Fz_rl * (W+DF) / Fz_total;
                Fz_rr = Fz_rr * (W+DF) / Fz_total;
                Fz_total = Fz_fl + Fz_fr + Fz_rl + Fz_rr;
            end

            if abs(Ay_new - Ay) < abs(Ay_new*.001) || abs(Ay_new) == 0
                converge = 1;
            else
                Ay = Ay_new;
                i = i+1;
            end

            i_mat(b,d) = i;
            Ax_mat(b,d) = Ax;
            Cn_mat(b,d) = Cn;
            Ay_mat(b,d) = Ay_new;
        end

        d = d+1;
    end
    b = b+1;
end


%plot diagram
figure()
xlabel('Lateral Acceleration Ay')
ylabel('Yaw Moment Cn')
zlabel('Longitudinal Accleration Ax')
hold on
```

```
grid on
for d = 1:size(deltas,2)
    l1 = plot3(Ay_mat(:,d),Cn_mat(:,d),Ax_mat(:,d),'b--');
end
for b = 1:size(betas,2)
    l2 = plot3(Ay_mat(b,:),Cn_mat(b,:),Ax_mat(b,:),'r');
end
legend([l1,l2],{'Constant Steer','Constant Vehicle Slip'})
hold off
```